Version of Record: https://www.sciencedirect.com/science/article/pii/S0883292722003158
Manuscript_89e8cd9a8a74fe525536af6bf24e7b27

Impacts of dissolved phosphorus and soil-mineral-fluid interactions on CO_2 removal through enhanced weathering of wollastonite in soils

Cameron Wood[a,1], Anna L. Harrison[a,b,2*], and Ian M. Power[c]

[a]Department of Geological Sciences and Geological Engineering, Queen's University, 36 Union Street K7L 3N6 Kingston, Canada

[b]School of Environmental Studies, Queen's University, 116 Barrie Street K7L 3N6 Kingston, Canada

[c]Trent School of the Environment, Trent University, K9L 0G2 Peterborough, Canada

[1] Present address: Department of Geoscience, University of Calgary, 2500 University Drive NW, T2N 1N4 Calgary, Canada (cameron.wood1@ucalgary.ca)

[2]Present address: Géosciences Environnement Toulouse (GET), Centre National de la Recherche Scientifique (CNRS), UMR 5563, Observatoire Midi- Pyrénées, 14 Avenue Edouard Belin, 31400 Toulouse, France (anna.harrison@get.omp.eu)

[*]Corresponding author : anna.harrison@get.omp.eu

Abstract

The weathering of silicate minerals removes carbon dioxide (CO_2) from the atmosphere over geologic timescales and is also investigated as an engineered strategy to mitigate climate change on decadal timescales. "Enhanced rock weathering" (ERW) is a carbon dioxide removal strategy that involves spreading of pulverized, highly reactive silicate rock at the Earth's surface such as within agricultural and natural soils. The rate and efficacy of ERW in agricultural soils to remove CO_2 is difficult to quantify owing to the complex geochemical environment including biological-mineral-fluid-atmosphere interactions and human interventions that occur. Column experiments containing wollastonite [$CaSiO_3$] and soils were conducted to investigate the geochemical processes that remove CO_2 during ERW, and to determine the potential impact of P-bearing fertilizers on CO_2 removal. Columns containing wollastonite, soil, or 8:1 soil-wollastonite mixtures were irrigated with de-ionized water or a 1×10^{-4} M K_3PO_4 solution. Analysis of column effluent concentrations indicated that P was rapidly removed from solution and retained within the columns, with little difference in weathering rate between columns irrigated with water and those receiving the K_3PO_4 solution. Bulk wollastonite weathering rates were significantly enhanced in the presence of soils compared to columns with wollastonite alone. Cation concentrations in effluent from columns with soil-wollastonite mixtures were strongly impacted by adsorption to soil surfaces, complicating efforts to estimate CO_2 capture. Based on wollastonite weathering rates estimated by Si release, a maximum of 255 kg CO_2 t^{-1} amendment yr^{-1} was captured in the soil-wollastonite mixture columns. The majority of CO_2 stored in the soil-bearing columns was most likely soil-generated rather than removed directly from the atmosphere. The results of this study indicate that adsorption to soils may limit the ability of P to enhance wollastonite weathering, that silicate weathering behaviour within soils differs substantially from that of pure mineral

phases, and that CO_2 budgets must be carefully constrained to assess the source of stored CO_2. Moreover, leachate concentrations of cations and HCO_3^- may not serve as accurate indicators of the extent of silicate weathering, at least over the short term, due to the numerous processes that control their concentrations in soils, such as sorption to soil components.

Keywords: wollastonite, enhanced rock weathering, CO_2 removal, mineral-soil interactions, negative emissions technologies

1. Introduction

Carbon dioxide removal (CDR) technologies will most likely be necessary alongside the reduction of CO_2 emissions to limit the global temperature increase to < 1.5 °C above pre-industrial levels and avoid the worst consequences of climate change (IPCC, 2018). Enhanced rock weathering (ERW) is a CDR technology that takes advantage of the natural process by which atmospheric CO_2 is removed during silicate mineral weathering but accelerates natural reaction rates to provide CO_2 removal on the much faster timescales that are necessary to address climate change (National Academies of Sciences, 2019; Schuiling and Krijgsman, 2006). ERW involves the dissolution of pulverized, high surface area alkaline earth metal-bearing silicate or hydroxide minerals in the presence of CO_2, which generates alkalinity, removes CO_2 from the atmosphere in dissolved form, and releases cations like Ca and Mg (Andrews and Taylor, 2019; Beerling et al., 2020; Daval, 2018; National Academies of Sciences, 2019; Power et al., 2013; Schuiling and Krijgsman, 2006). ERW captures CO_2 in dissolved form as carbonate alkalinity that is transported eventually to the oceans, and in some cases also stores CO_2 in solid form as carbonate minerals (e.g., calcite [$CaCO_3$]) (National Academies of Sciences, 2019; Power et al., 2013).

The application of alkaline silicate minerals to agricultural fields as soil amendments is one method for implementing ERW (Zhang et al., 2018). The acidic root exudates emitted by some crops may also promote silicate dissolution, releasing additional nutrients for plant consumption (Haque et al., 2019). The high dissolution rate, high Ca content per unit mass, and simple chemical composition of wollastonite [$CaSiO_3$] make it an attractive option both for CO_2 storage and for studies of silicate dissolution rates and mechanisms (Haque et al., 2019; Schott et al., 2012). In the case of wollastonite weathering, CO_2 removal occurs according to Equation 1.

$$CaSiO_3 + 2CO_2 + 3H_2O \rightarrow Ca^{2+} + H_4SiO_4 + 2HCO_3^- \quad \textit{Equation 1}$$

From the alkalinity and Ca released from the silicate minerals, carbonate minerals such as calcite can form (according to Equations 2 and 3):

$$HCO_3^- \leftrightarrow CO_3^{2-} + H^+ \quad \textit{Equation 2}$$

$$Ca^{2+} + CO_3^{2-} \leftrightarrow CaCO_3 \quad \textit{Equation 3}$$

In cases where silicate weathering occurs due to an acid other than CO_2, such as nitric acid from N-bearing fertilizers, no atmospheric CO_2 is stored (Andrews and Taylor, 2019; Hartmann et al., 2013). However, the impacts of ligands in soil pore waters, like dissolved organics and phosphorus, on CO_2 removal during wollastonite dissolution are not well understood. Microbial activity within soils can also result in release of CO_2 to the atmosphere as organic C is consumed and expelled as CO_2, though the organic C may initially have been atmospheric CO_2. Some of the CO_2 released by biological processes could be retained as dissolved inorganic carbon (DIC), resulting in no net change in atmospheric CO_2. The many interrelated processes that occur during ERW in soils make tracing the source and fate of CO_2 and thus quantifying the efficacy of CDR during ERW in soils highly complex.

It has been estimated that by 2050, global agricultural adoption of ERW could remove up to 2.0 Gt of CO_2 per year (Beerling et al., 2020). In addition to CO_2 capture, silicate soil amendments could potentially provide further environmental and agricultural benefits. Silicate mineral amendments can combat soil acidification by raising soil pH and supplying Ca, Mg, Si, and various micronutrients to soils (Harley and Gilkes, 2000). Soil Si depletion is a concern in areas of intensive agriculture and could necessitate direct Si fertilization (Tubana et al., 2016). Silicate soil amendments thus have the potential to simultaneously enhance soil productivity and remove atmospheric CO_2 (Haque et al., 2019).

Experimental studies investigating the dissolution of silicate soil additives have used olivine [Mg_2SiO_4] (Pogge von Strandmann et al., 2022; Renforth et al., 2015), basalt (Anda et al., 2013; Anda et al., 2015; James et al., 2020; McDermott et al., 2019; Ten Berge et al., 2012; Kelland et al., 2020), dolerite (Manning et al., 2013), dunite (Amann et al., 2020), and wollastonite (Haque et al., 2020; Haque et al., 2019; Peters et al., 2004; Shao et al., 2016; Taylor et al., 2021). In a large-scale field experiment where pelletized wollastonite was applied to a 11.8 ha watershed, a 50% increase in stream water concentrations of Ca and Si over a period of 1 to 2 years was observed (Peters et al., 2004; Shao et al., 2016). An upper estimate for the CO_2 captured by wollastonite weathering in this watershed was calculated to be 0.22 kg CO_2 t amendment^{-1} yr^{-1} (Taylor et al., 2021). Bench-scale experimental studies showed that in the presence of legumes, wollastonite weathering can result in CO_2 storage by $CaCO_3$ precipitation that is enhanced up to 10 times compared to soils without wollastonite (Haque et al., 2019). A field study revealed up to 224-4800 kg CO_2 t amendment^{-1} yr^{-1} was sequestered as solid inorganic carbon (SIC) in a wollastonite-amended field growing leafy vegetables, with the greatest CO_2 sequestration achieved in a field that had received both wollastonite and monoammonium phosphate fertilizer (Haque et al., 2020).

Phosphorus-bearing fertilizers are commonly applied in agricultural settings, where interactions between dissolved phosphorus and mineral soil amendments (such as wollastonite) may take place. In a study that supplied 118 kg P_2O_5 ha^{-1} yearly to soils, soil porewater P concentrations up to 0.170 mM were measured (Sigua et al., 2017). This is near to or less than application rates that have been recommended for certain crops in some U.S. states (Rosen et al., 2014). This suggests that in many agricultural areas, soil porewater P concentrations may be in excess of the 0.03 mM $H_2PO_4^{2-}$ shown to triple the dissolution rate of wollastonite at 25 °C and neutral pH (Pokrovsky et al., 2009). If soil porewater P

significantly enhances the dissolution of wollastonite, it could represent an important factor affecting release rates of Ca and Si, impacting CO_2 storage from ERW in soils. Although the potential impact of N-bearing fertilizers on ERW has been previously discussed (Andrews and Taylor, 2019; Hartmann et al., 2013), the impact of P-bearing fertilizers on ERW rates is yet to be fully understood. Prior research on the interactions between phosphorus and silicate minerals within soils has largely focused on the availability of P for uptake by plants (Mkhonza et al., 2020; Jakobsen, 1979). Silicon was found to compete with P for soil adsorption sites and to increase the availability of P in solution (Lee and Kim, 2007; Obihara and Russell, 1972; Roy et al., 1971). Geochemical modeling on the watershed scale has also indicated that wollastonite could potentially aid in remediation of P-rich agricultural runoff through formation of hydroxylapatite [$Ca_5(PO_4)_3(OH)$] (Hayder et al., 2019). However, the potential of P-bearing fertilizers to accelerate the dissolution of silicates within soils and to contribute to ERW and CDR has not previously been investigated, to the best of our knowledge. In this study, a series of small-scale (10 cm tall by 1.95 cm diameter and 30 cm^3 volume) laboratory column experiments were conducted to evaluate the influence of soil-fluid-mineral interactions and the presence of dissolved P on the weathering of wollastonite and CO_2 removal. The objectives of this study were: 1) to evaluate the influence of soil-fluid-mineral interactions on elemental fluxes during ERW, 2) to quantify the weathering rates of wollastonite in soils, and the impact of the presence of P in particular, and 3) to contribute to the understanding of processes impacting CO_2 removal during ERW in soils.

2. Materials and Methods

2.1. Experimental design

Wollastonite used in the column experiments was obtained from the Canadian Wollastonite Mine located 34 km northeast of Kingston, Ontario, Canada. The wollastonite was sieved to a grain size of 62.5 – 125.0 µm and sonicated in ethanol to remove fine particles. Local potting soil with no added fertilizer was purchased from a garden center in Kingston, Ontario. This soil was an in-house blend which contained visible fragments of wood and plant matter. The soil was air dried prior to analysis and column construction. After drying, the soil was homogenized by hand, and any visible large pebbles or pieces of plant matter were removed. Ten columns were constructed using 30 mL cylindrical syringes filled to the 30 mL mark (10 cm height with 1.95 cm diameter) (Table 1). Two of these columns were filled with wollastonite (32.8 and 34.6 g), two with soil (12.44 and 12.19 g), and six with an 8 to 1 mixture of soil and wollastonite (approximately 13.81 g total). Columns containing the wollastonite-soil mixture were run in triplicate to assess impacts of heterogeneity in the soil-wollastonite mixture. An 8 to 1 ratio of soil to wollastonite employed in a previous study of wollastonite weathering in agricultural soils was calculated to result in a positive saturation index for calcite (Haque et al., 2019). To inhibit discharge of solids, 63 µm nylon mesh was placed at the base of each column. Tygon tubing with a 4.76 mm internal diameter was affixed to the bottom of each syringe to direct flow to a fluid collection container. Masses of the empty columns, columns filled with dry solids, and columns filled with water saturated solids were recorded. Water was added gradually using a transfer pipette. Columns were considered fully saturated when the mass of the column after added water was no longer present on top of the soil was equal to the column mass prior to the most recent addition of water. Column initial conditions are provided in Table 1. A schematic of the column experiment is provided in Figure 1. The following nomenclature is used throughout the manuscript: Wollastonite-Water is referred to as WW,

Wollastonite-P as WP, Soil-Wollastonite as SW, Soil-P as SP, Mixture-Water replicates as MW (1, 2, 3), and Mixture-P replicates as MP (1, 2, 3).

Table 1. Medium, solution, mass, and pore volume data for column experiments

Column[a]	Medium	Solution[b]	Dry Mass (g)[c]	Wet Mass (g)[c]	Pore Volume (mL)[c]
WW	Wollastonite	Water	32.80	48.37	15.57
WP	Wollastonite	K_3PO_4	34.60	50.52	15.92
SW	Soil	Water	12.44	30.3	17.86
SP	Soil	K_3PO_4	12.09	30.75	18.66
MW 1	Soil-Wollastonite	Water	13.20	32.91	19.71
MW 2	Soil-Wollastonite	Water	12.81	34.37	21.56
MW 3	Soil-Wollastonite	Water	13.81	34.36	20.55
MP 1	Soil-Wollastonite	K_3PO_4	14.52	34.47	19.95
MP 2	Soil-Wollastonite	K_3PO_4	14.28	34.06	19.78
MP 3	Soil-Wollastonite	K_3PO_4	14.26	34.77	20.51

[a]Soil-water (SW), Soil-P (SP), Wollastonite-Water (WW), Wollastonite-P (WP), Mixture-Water (MW), Mixture-P (MP) where mixture indicates an 8:1 mixture of soil and wollastonite.
[b]De-ionized water was applied to columns receiving water and a 1×10^{-4} M K_3PO_4 (3.096 mg L^{-1} P) solution was applied to columns receiving K_3PO_4.
[c]Dry and wet masses are initial masses with Pore Volume = Wet Mass – Dry Mass.

Irrigation of the columns was carried out daily during the first week, then every other day for the remainder of the month-long experimental period. Transfer pipettes were used to simulate rain and avoid disturbing the solids. A volume of 21 mL, equivalent to at least one pore volume, was used for each irrigation event. A separate aliquot of fluid was used for each column, with the mass of the container measured before and after irrigation to verify the mass of fluid added to each column. Half of the columns (one wollastonite, one soil, three mixture) were irrigated with de-ionized water. The other half of the columns were irrigated with a 1×10^{-4} M K_3PO_4 (3.096 mg L^{-1} P) solution, which was acidified to pH 6 (equivalent to the pH of the deionized water) with < 1 µL 1 N HCl.

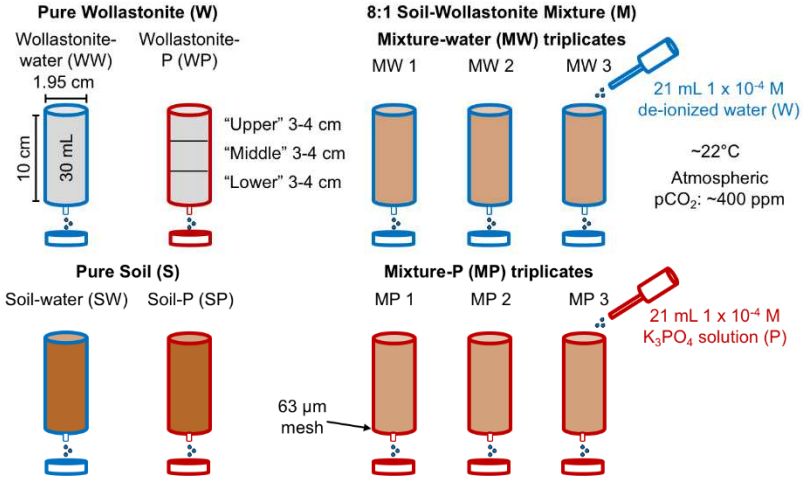

Figure 1. Column experiment schematic. The masses of wollastonite present in columns were 32.8 g (WW), 34.6 g (WP), 1.47 g (MW 1), 1.42 g (MW 2), 1.54 g (MW 3), 1.61 g (MP 1), 1.59 g (MP 2), and 1.58 g (MP 3).

2.2. Sampling Protocol

Effluent discharged rapidly as the columns were irrigated and the entire volume of effluent was collected during each irrigation period. Effluent vials were weighed before and after sample collection such that the mass of fluid discharged at each step could be determined. The mass of each column was also measured before and after each irrigation. An aliquot of 6 mL of the irrigation effluent was filtered using a 0.20 µm polyethersulfone (PES) syringe filter and acidified to 2% HCl for analysis of cation and P concentrations. The pH of the unacidified effluent was measured using a WTW portable pH meter model pH 3310 with a SenTix 41 probe which was calibrated daily using pH 4.01, 7.00, and 9.18 buffer solutions. Two milliliters of unacidified, unfiltered effluent was collected in tubes without head space for P and organic/inorganic carbon measurement. After the final irrigation, solids from each of the columns were collected and material from each of the upper, middle, and lower 3-4 cm of each column were separated. The solids in each of the

upper, middle, and lower sections was then homogenised. The wet masses of each wollastonite, soil, and mixture segment were approximately 13, 5, and 6 g, respectively. The solids were dried at room temperature and reweighed after drying to evaluate the saturated water content. Solids were analyzed by X-ray diffraction (XRD) and scanning electron microscopy (SEM).

2.3. Solid Analyses

Brunauer-Emmett-Teller (BET) surface area of the cleaned wollastonite was analyzed by Kr adsorption using a Micromeritics Tristar II plus. Analysis of the wollastonite yielded a surface area of 0.142 m^2/g. The mineralogical composition of the initial solids and select samples after the experiments was analyzed using XRD. Dry aliquots of samples were ground using an agate mortar and pestle with anhydrous ethanol and mounted as a slurry on zero-diffraction quartz plates. The XRD data were collected using a Bruker D2 Phaser diffractometer using a 0.02° step size over a range of 5–80° 2θ at 2 s per step. The patterns were collected using a Lynx Eye XE-T detector coupled with a 0.6 mm divergence slit, and incident and diffracted beam Soller slits. A fine-focus Cu X-ray tube, operated at 30 kV and 10 mA, was used to generate X-rays. Mineral phases were identified using DIFFRACplus EVA V4.3 a search-match software obtaining crystal structure data from the International Center for Diffraction Data PDF 2+ 2020. Organic and inorganic carbon content of solids was analyzed at the Agriculture and Food Laboratory at Guelph University, using a Leco CN828 apparatus. This instrument provides elemental analysis of nitrogen, total carbon, and inorganic carbon (IC) by ashing the sample at 475 °C for 3 h prior to carbon analysis using catalytic combustion (950 °C), separating out the desired measurement components from foreign gases, and analyzing using thermal conductivity detection and infra-red detection. Organic carbon is calculated from the

subtraction of the inorganic carbon result from the total carbon result. The limit of carbon detection in soils was 0.005 % for inorganic and total carbon.

Initial solids and certain reacted solid samples were examined using an FEI Quanta 650 Field Emission Gun (FEG) Environmental Scanning Electron Microscope (ESEM). Samples were analyzed under high vacuum mode with a working distance of 9-12 mm, voltage of 5.00 kV, and a secondary electron detector.

2.4. Fluid Analyses

The Ca, Si, and K concentrations in fluid samples from columns WW, WP, SW, SP, MW 1, and MP 1 were analyzed using an iCAP^{TM} TQs triple quadrupole inductively coupled plasma mass spectrometer (TQ ICP-MS). Isotopes were measured in three modes: single quadrupole with no cell gas, single quadrupole in KED mode (He collision gas) and triple-quadrupole with O_2 as the reaction gas, utilizing mass shifting. The concentrations of Ca, Si, K, P, Mg, Fe, Sr, and Na in select samples from the above columns as well as samples from columns MW 2, MW 3, MP 2, and MP 3 were measured with an iCAP^{TM} PRO inductively coupled plasma optical emission spectrometer (ICP-OES). The ICP-OES was optimized daily using a multi-element test solution consisting of 10 ppm P, 5 ppm K and Ni, 1 ppm Al, Cu, and Mn, and 0.2 ppm Ba, Ca, Mg, and Zn. The optimization procedure included optimization of gas flows (nebulizer, auxiliary and cool gas), torch position, optics alignment and RF power. The certified reference materials (CRMs) used for both TQ ICP-MS and ICP-OES were SLRS-6, AQUA-1, and NIST1643f. Standard deviation and standard error values of CRMs are provided in Table S1 in the Supplementary Materials (SM). Detection limits of Ca and Si by ICP-OES were 0.018 and 0.002 ppm, respectively, and the detection limits of Ca and Si by TQ ICP-MS were 0.0002 and 0.03 ppm respectively.

242 Total P concentrations of samples from columns WW, WP, SW, SP, MW 1, and MP
243 1 were measured by the Analytical Services Unit at Queen's University, Canada using a
244 Seal AutoAnalyzer under computer control using AACE version 6.05 software by Seal
245 Analytical, Inc. Wisconsin, USA. Samples were delivered from a Bran+Luebbe XY-2
246 Autosampler system, supplied by Seal. Detection by absorbance was carried out at 660 nm,
247 on a Seal AutoAnalyzer 3 High Resolution Digital Colorimeter. Soluble phosphorus in
248 samples was reacted with ammonium molybdate in the presence of antimony, diluted with
249 acid, then reduced with ascorbic acid to yield the detected blue-coloured complex.
250 Dissolved organic and inorganic carbon concentrations (DOC and DIC,
251 respectively) were measured using a Shimadzu TOC-V_{CSN} analyzer. Samples were first
252 acidified to release CO_2 from dissolved inorganic carbon. After DIC removal, the sample
253 was heated to 680 °C to transform dissolved organic carbon to CO_2, which was quantified
254 as non-purgeable organic carbon with an infrared detector. The quantification limit for DIC
255 was 0.57 ppm, and for DOC was 0.47 ppm. Blanks of two samples of filtered deionized
256 water were analyzed and their average DIC and DOC concentration subtracted as
257 background from samples. Uncertainty in DIC and DOC concentration was better than 1.25
258 ppm and 1.98 ppm, respectively. However, the presence of solid organic material observed
259 in some samples may impact the precision of DOC results.

260 *2.5. Speciation calculations*

261 Aqueous speciation of column leachate and saturation indices of mineral phases
262 that could dissolve or precipitate were determined using PHREEQC Interactive v. 3.4.0
263 with the LLNL database (Parkhurst and Appelo, 2013). Data input to PHREEQC consisted
264 of the pH and all measured elemental concentrations for each modeled timepoint, including
265 DIC and concentrations measured by TQ ICP-MS, ICP-OES, and digital colorimetry.
266

3. Results

3.1. Characterization of Solids

Wollastonite was the only phase detected by XRD in the initial wollastonite samples. The initial wollastonite contained 0.026% inorganic and 0.033% organic C. The initial soil was composed of albite ($NaAlSi_3O_8$), quartz (SiO_2), and minor amounts of calcite ($CaCO_3$) and dolomite [$CaMg(CO_3)_2$] in addition to organic matter. Calcite and dolomite were not detected by XRD in the soil-wollastonite mixture, suggesting they were present below the detection limit (~ 0.5 wt.%). Wollastonite, albite, and quartz were the only minerals detected by XRD in the initial soil-wollastonite mixture (Figure S1 in (SM)).

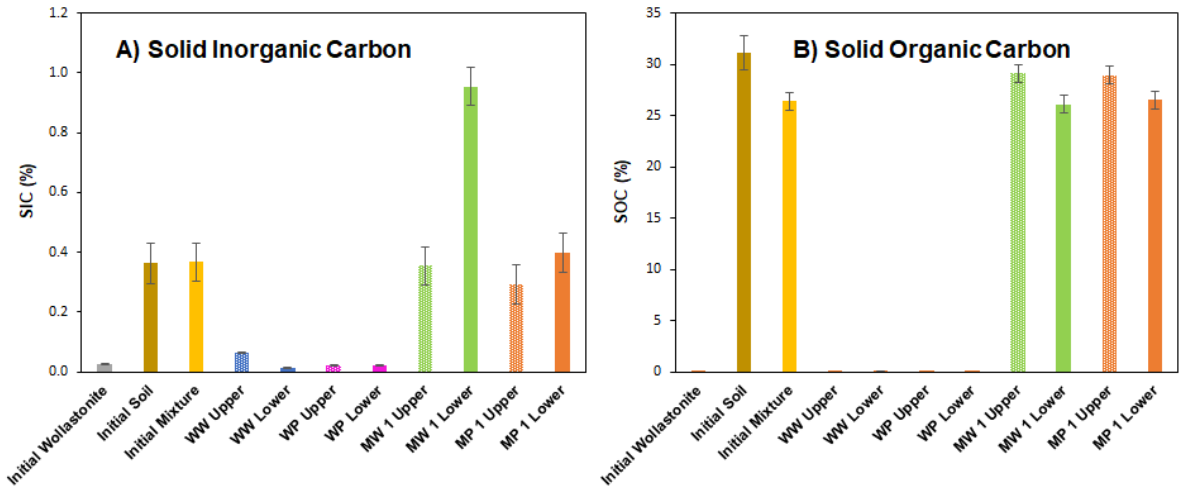

Figure 2. Solid inorganic (SIC) and organic carbon (SOC) contents of initial and reacted column contents. Error bars indicate standard deviation (n = 3) of initial sample measurements for each material. Abbreviations are defined as: Wollastonite-Water (WW), Wollastonite-P (WP), Mixture-Water (MW), and Mixture-P (MP) where mixture indicates an 8:1 mixture of soil and wollastonite. Upper and lower refers to the upper and lower 3-4 cm of each column, respectively.

Although it is possible that clay minerals were present in the initial soil, they were not present in sufficient quantity to be detected by XRD. Precise abundances of minerals could not be determined due to analytical limitations related to the large quantity of X-ray amorphous material. Organic and inorganic C contents of the initial wollastonite, initial soil, and initial mixture were each measured for triplicate aliquots of the initial material to assess

heterogeneity in C content (Table 2). The soil was rich in organic C (31.1 ± 1.6%, n=3) (Figure 2) and contained 0.363 ± 0.067% (n=3) inorganic C prior to reaction. Less solid C was detected in the mixture than in the soil, owing to its wollastonite content, with average total solid C contents of 0.042 ± 0.012, 26.7 ± 0.8, and 31.4 ± 1.6% (n=3) for the initial wollastonite, initial mixture, and initial soil, respectively.

Table 2. Inorganic and organic carbon contents of solids

Sample[a]	% Inorganic Carbon	% Organic Carbon	% Total Carbon
Initial Wollastonite[b]	0.025 ± 0.002	0.018 ± 0.011	0.042
Initial Soil[b]	0.363 ± 0.067	31.1 ± 1.6	31.4
Initial Mixture[b]	0.367 ± 0.064	26.4 ± 0.9	26.7
WW Upper	0.064 ± 0.002	0.018 ± 0.011	0.083
WW Lower	0.012 ± 0.002	0.030 ± 0.011	0.043
WP Upper	0.023 ± 0.002	0.011 ± 0.011	0.035
WP Lower	0.023 ± 0.002	0.016 ± 0.011	0.039
MW 1 Upper	0.355 ± 0.064	29.1 ± 0.9	29.5
MW 1 Lower	0.955 ± 0.064	26.1 ± 0.9	27.0
MP 1 Upper	0.293 ± 0.064	28.9 ± 0.9	29.2
MP 1 Lower	0.399 ± 0.064	26.5 ± 0.9	26.9

[a]Wollastonite-Water (WW), Wollastonite-P (WP), Mixture-Water (MW), Mixture-P (MP) where mixture indicates an 8:1 mixture of soil and wollastonite. Upper and lower refers to the upper and lower thirds of columns, respectively, which were each ~3.3 cm depth. Samples not labelled "initial" indicate final values. Detection limit for inorganic and organic carbon was 0.005%.
[b]Values presented are an average (n = 3) with error values indicating standard deviations. Standard deviations of the triplicate measurements of initial materials are also used for final solids as there was insufficient final solid for triplicate analyses.

After the experiments, no secondary phases nor substantial changes to initial mineralogy were evident in the reacted solids based on XRD results (Figure S2 in SM). Dolomite was detected in the reacted mixture columns, despite not being detected in the initial mixture, suggesting it may be heterogeneously distributed (Figure S2 in SM). Calcite remained in all soil and mixture columns after the experiments (Figure S2 in SM). A decrease in the relative intensity of wollastonite peaks in the reacted mixtures compared to the initial mixtures may reflect the dissolution of wollastonite within the column.

All wollastonite column segments exhibited a decrease in organic C relative to the initial wollastonite at the end of the experiments (Table 2). The upper section (upper 3-4

312 cm) of column WW showed a marked increase in solid inorganic C (SIC) from 0.026 % ±
313 0.002% to 0.064 % ± 0.002%, but an increase was not observed in either the lower section
314 (lower 3-4 cm) of WW or in solids from WP, for which a modest decrease in SIC was
315 observed. Organic C content of the mixture columns varied, with the upper portions of MW
316 1 and MP 1 containing 2.5-2.7 % more organic C than the initial mixture and the lower
317 portions within uncertainty of the initial mixture (Table 2). This could be caused by
318 heterogeneity in the initial soil used in the mixtures, although the difference in the upper
319 column portions exceeds the uncertainty of the triplicate analyses. The only significant
320 change in SIC in a mixture column segment was observed in the lower portion of MW 1,
321 which showed an increase from 0.294 to 0.955 % (Table 2), which suggests either some
322 accumulation of SIC or potentially large heterogeneity in initial soil carbonates resulting in
323 different initial SIC between mixture columns. However, such substantial heterogeneity
324 was not observed in the measurement of triplicate aliquots of either the initial soil or the
325 initial mixture.
326 Scanning electron microscopy showed that the initial wollastonite had smooth
327 surfaces (Figure 3 A). Soils were of irregular texture with a range of constituents
328 amalgamated into clumps (Figure 3 B). Wollastonite from columns irrigated with water
329 (Figure 4 A) or K_3PO_4 (Figure 4 B) displayed rougher surfaces than the initial material,
330 indicative of dissolution. The wollastonite surfaces were observably rougher in the mixture
331 columns, with more fractures and pits (Figure 4 D, E, F), than in the wollastonite columns
332 after reaction (Figure 4 A, B, C), likely reflecting a greater extent of weathering. Surface
333 features consistent with secondary precipitates were visible in the upper portion of MP 1
334 (Figure 4 E) and in the lower portion of MW 1 (Figure 4 D). The precipitates could not be
335 identified based on the images, however, and were not of sufficient quantity to be detected
336 by XRD although an increase in the SIC content of MW 1 was observed.

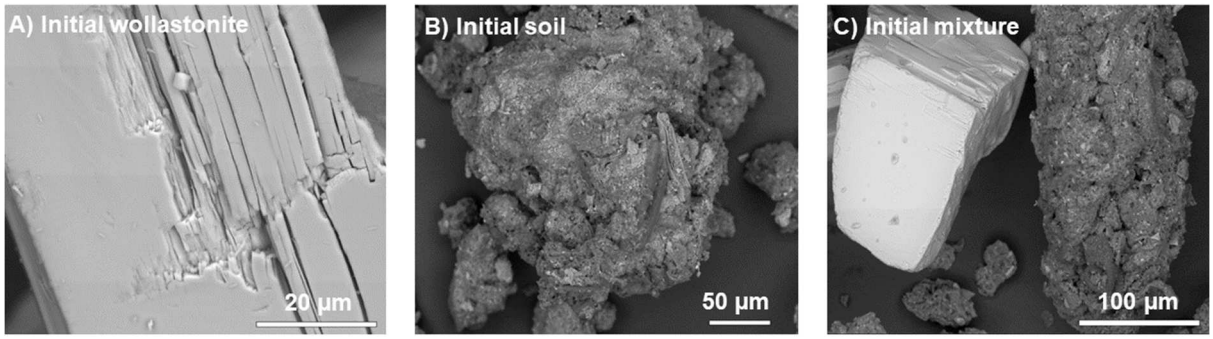

Figure 3. Scanning electron microscope images of initial wollastonite (A), initial soil (B), and soil-wollastonite mixture (C).

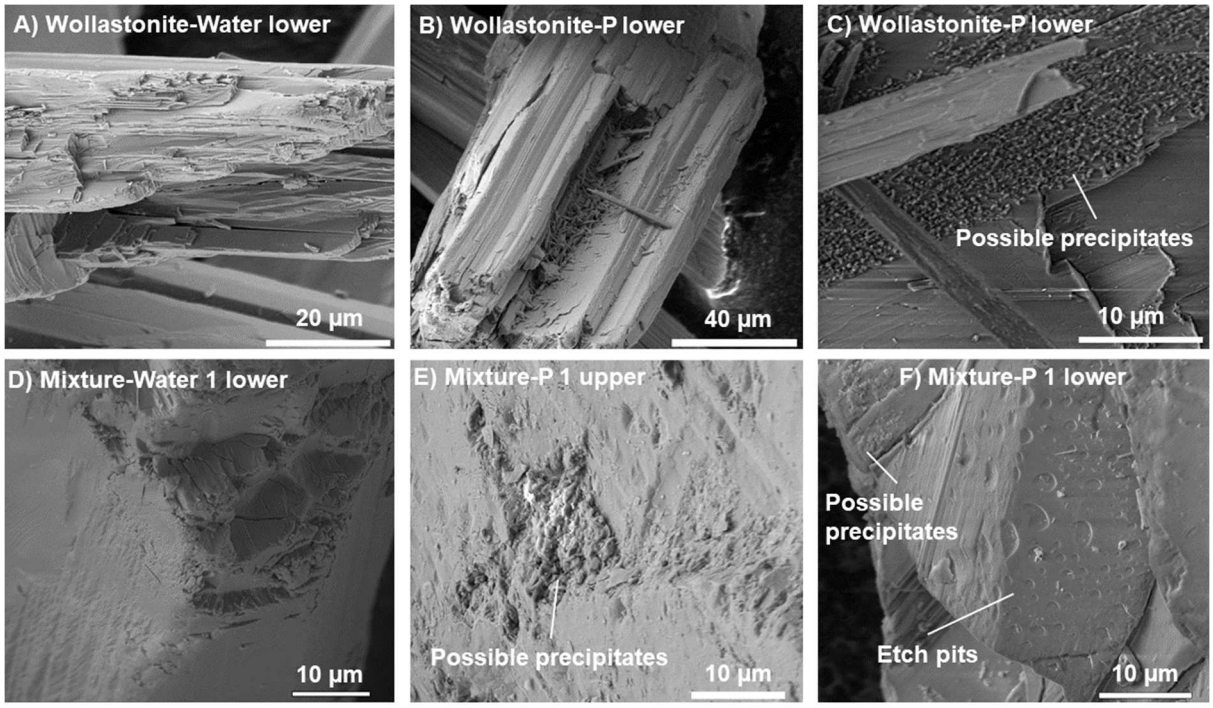

Figure 4. Scanning electron microscope images of Wollastonite-Water (WW) lower (A), Wollastonite-P (WP) lower (B), Wollastonite-P lower (C), Mixture-Water 1 (MW 1) upper (D), Mixture-P 1 (MP 1) upper (E), and Mixture-P 1 lower (F), where mixture indicates an 8:1 mixture of soil and wollastonite. Upper and lower refer to the upper and lower 3-4 cm of the columns, respectively.

3.2. Trends in fluid composition

In all cases, effluent pH values were higher than the input solution pH value of 6 (Figure 5). Effluent pH values were consistently 1.0 to 1.7 units higher in the wollastonite columns compared to mixture columns and 1.4 to 2.3 units higher than the soil columns. A difference in pH between columns receiving water and K_3PO_4 was only apparent in the soil columns. Effluent pH from the WW and WP columns was between 8.91 to 9.40 and

remained fairly constant throughout the experiment (Figure 5 A). The pH values of effluent from column WP were slightly higher than for WW at all but one time point. The effluent from the SW column had a consistently higher pH than the SP column effluent, with each beginning near pH 8 at the beginning of the experiment before declining to approximately stable values of ~7.5 and 6.9, respectively after ~180 h (Figure 5 A). Mixture column pH values were ~8 throughout the experiment for the columns receiving water (Figure 5 A).

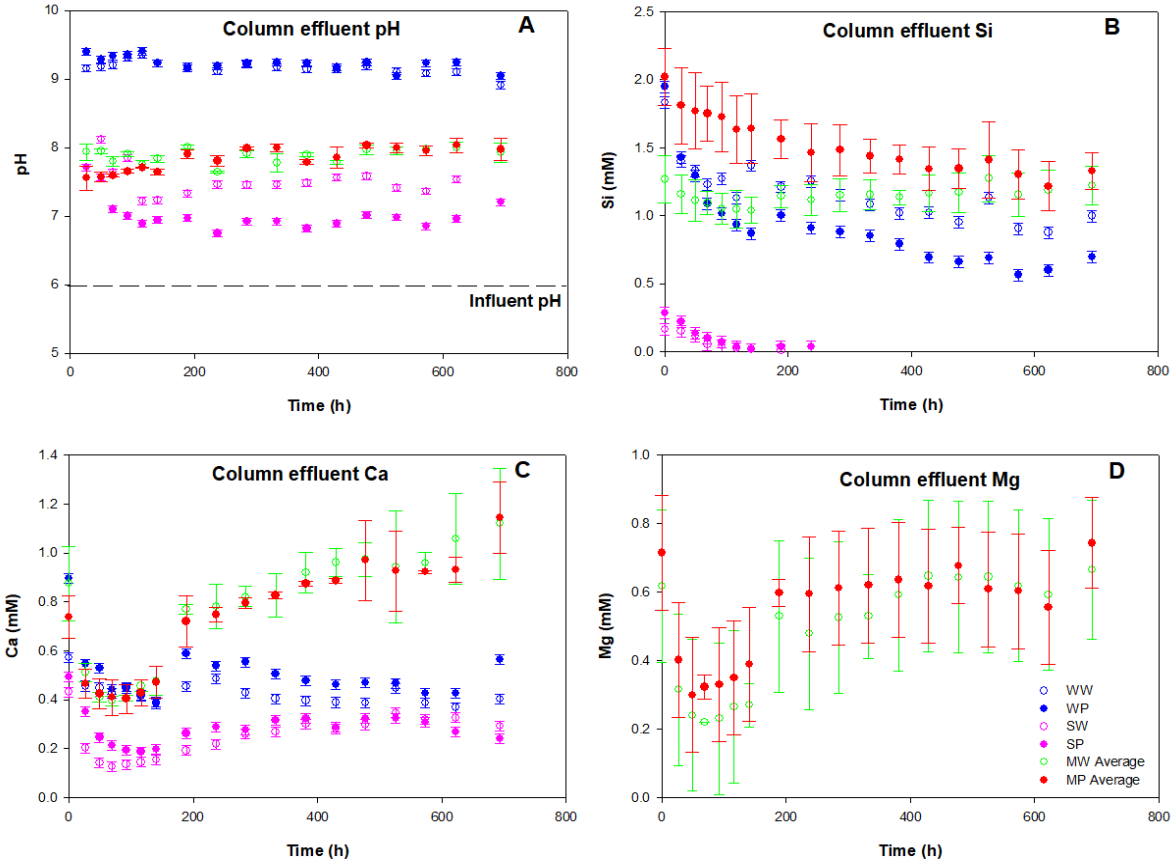

Figure 5. pH values of column effluent (A), Si concentrations of column effluent (B), Ca concentrations of column effluent (C). Mixture column data is presented as an average of concentrations from three replicate columns. Error bars for non-replicated columns indicate the maximum standard deviation (SD) of triplicate samples (maximum SD was used where only one sample was analyzed for a time point) and error bars for replicated columns indicate the SD of concentrations in samples taken at the same time point for replicate columns. WW (Wollastonite-Water), WP (Wollastonite-P), Soil-Water (SW), Soil-P (SP), MW (Mixture-Water), MP (Mixture-P), where mixture indicates an 8:1 mixture of soil and wollastonite.

370 Mixture columns receiving the K_3PO_4 solution began near pH 7.5 before increasing
371 to ~8 by ~180 h and remaining stable at this pH value for the remainder of the experiment
372 (Figure 5 A). The pH values of columns SW and SP were 0.2-0.7 and 0.5-1.2 pH units
373 lower than the respective mixture columns receiving the same input solution past 150 h.
374 Although effluent Si concentrations were generally greater in the mixture columns
375 compared to the wollastonite columns, effluent Si trends were comparable in the
376 wollastonite and mixture columns, exhibiting a similar decline over time and with little
377 influence of P documented. On the other hand, soil effluent Si concentrations were lower
378 and declined to the detection limit by 285 h (Figure 5 B). Dissolved Si concentrations in
379 effluent from WW and WP columns were nearly 2 mM after ~1 h but declined for the
380 remainder of the experiment to a minimum of 0.88 mM for column WW and 0.56 mM for
381 column WP, respectively (Figure 5 B). Column WW exhibited higher Si concentrations
382 compared to column WP throughout the majority of the experiment (Figure 5 B). Silicon
383 output from all the MW columns was reasonably constant throughout the experimental
384 duration, with values between 1-1.5 mM (Figure 5 B). The MP columns effluent initially
385 exhibited Si concentrations greater than 2 mM, but the Si concentrations declined
386 throughout the experiment to similar values as the MW columns by 600 h (Figure 5 B).
387 Calcium concentrations in the wollastonite column effluent were initially 0.57 and
388 0.90 mM after ~ 1 h but declined to a stable value between 0.36 and 0.58 mM in the WW
389 and WP column effluents, respectively. Effluent from column WP consistently displayed
390 higher Ca concentrations than effluent from column WW, in contrast to the behaviour of Si
391 between these columns (Figure 5 C). Initial Ca concentrations in the soil column effluent
392 were 0.43 and 0.49 mM for columns SW and SP, respectively, but declined to ~0.2 mM
393 within 100 h before gradually increasing to a fairly stable plateau at 0.27-0.33 mM by 500
394 h. Calcium concentrations in the mixture columns showed a similar trend as the soil

columns over time, with a rapid decline to a minimum followed by a more gradual increase after 100 h. The Ca concentrations in the mixture columns were generally greater than those in the soil columns and reached higher values than in the pure wollastonite columns. In both the soil and mixture columns, there was no clear impact of irrigation with water versus K_3PO_4 on Ca concentrations.

Sodium and Mg concentrations were only measured for columns MW 2, MW 3, MP 2, and MP 3. Magnesium concentrations in the mixture columns exhibited similar trends to Ca concentrations though concentrations were lower overall. Magnesium concentration in all measured columns declined to ~0.2-0.4 mM in the first 100 h, then increased to a stable value of 0.6 mM by 400 h. Sodium concentrations decreased from ~2 mM at the start of the experiment to < 0.1 mM by 400 h.

The total moles of Ca and Si exported from the wollastonite columns was comparable to the quantity exported from the mixture columns despite a much smaller amount of wollastonite present in the mixture columns (Table 3). Despite differences between the wollastonite columns receiving water and the K_3PO_4 solution being apparent, the effects on Ca and Si were opposite, making it difficult to discern whether dissolution of wollastonite was enhanced in the presence of P. The impact of P on the mixture columns also differed for Ca and Si, with more Ca discharged from the mixture columns receiving water and more Si discharged from the mixture columns receiving the K_3PO_4 solution. This impact is opposite from that observed in the wollastonite columns. Column WW discharged 43 % more Si and 13 % less Ca than column WP normalized to initial wollastonite mass. On average, mixture columns receiving water discharged 9 % more Ca than mixed columns receiving K_3PO_4, but the mixture columns with P discharged 13 % more Si than those with water. The mixture columns receiving water and K_3PO_4, respectively, discharged an average of 202 % and 332 % more Ca and an average of 243 % and 196 % more Si,

normalized to initial wollastonite mass, than the respective wollastonite columns receiving the same inlet fluid. In all columns containing wollastonite, the Si:Ca ratio of column effluent was > 1 throughout the experiment, except in samples from column MW 2 after 600 h. The Si:Ca ratio of the mixture columns and of column WP declined over time, approaching 1:1 by the end of the experiment (Figure S3 in SM).

Table 3. Total calcium and silicon fluxes from the columns

Column[a]	mmol Ca Exported	% Ca Exported[b]	mmol Si Exported	% Si Exported[b]
WW	0.155	0.06	0.423	0.15
WP	0.183	0.06	0.312	0.11
SW	0.086	N/A	0.010	N/A
SP	0.101	N/A	0.052	N/A
MW 1	0.260	2.06	0.349	2.77
MW 2	0.283	2.31	0.465	3.80
MW 3	0.240	1.82	0.431	3.26
MP 1	0.226	1.63	0.466	3.36
MP 2	0.272	1.99	0.622	4.56
MP 3	0.333	2.44	0.632	4.63

[a]Wollastonite-Water (WW), Wollastonite-P (WP), Soil-Water (SW), Soil-P (SP), Mixture-Water (MW), Mixture-P (MP) where mixture indicates an 8:1 mixture of soil and wollastonite.
[b]Percent values are reported relative to initial moles of Ca or Si in wollastonite present in the column.

In all columns receiving K_3PO_4, less than 22 % of P added to columns through irrigation was discharged. In all experiments, the effluent remained well below the influent concentration throughout the experimental duration (Figure 6). There was some initial P discharge from the MW 2 and 3 columns, and P concentration in the MP 2 and 3 column effluent gradually increased over time. Phosphorus detected in effluent from soil columns was near the detection limit. Phosphorus concentrations for the MW 2 and 3 and MP 2 and 3 columns were measured by TQ ICP-MS as opposed to digital colorimetry, which was used for P concentrations in columns WW, WP, MW 1, and MP 2. The detection limit for P is lower with ICP-MS, at 0.00016 mM as opposed to 0.0032 mM for digital colorimetry. This is likely why P was detected in the effluent from the mixture columns but not the soil columns.

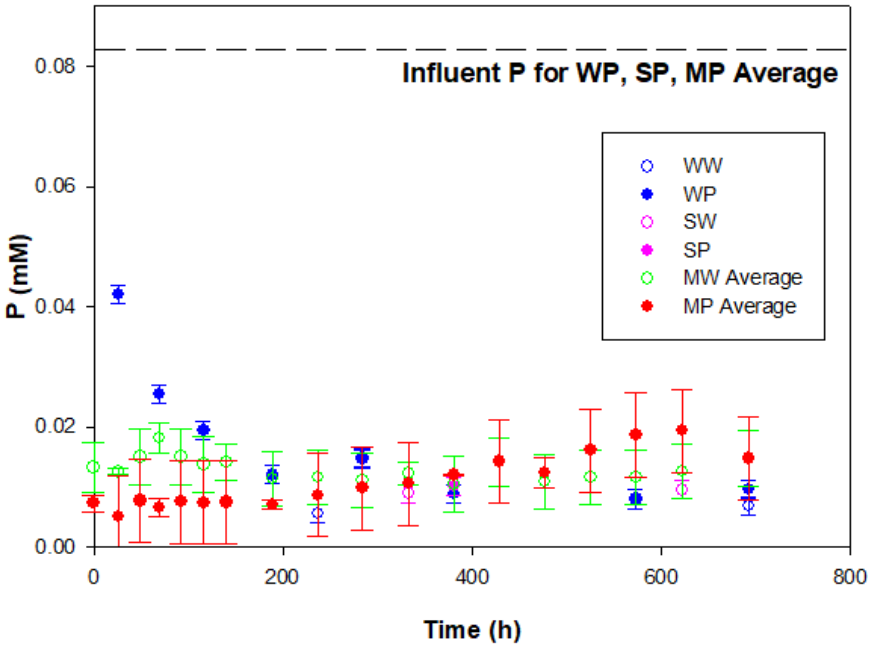

Figure 6. Dissolved P concentrations column effluent. Mixture column data is presented as an average of three replicate columns. Error bars for non-replicated columns indicate the maximum standard deviation (SD) of triplicate samples (maximum SD was used where only one sample was analyzed for a time point) and error bars for replicated columns indicate the SD of concentrations from column samples taken at the same time point for replicate columns. WW (Wollastonite-Water), WP (Wollastonite-P), Soil-Water (SW), Soil-P (SP), MW (Mixture-Water), MP (Mixture-P), where mixture indicates an 8:1 mixture of soil and wollastonite.

The concentration of K in effluent from the WP column was approximately equal to the influent concentration of 0.3 mM throughout the experiment (Figure S4A in SM), but K concentrations in column SP and mixture columns receiving the K_3PO_4 solution were substantially lower than in the influent. In the SP column, K concentrations were relatively constant near 0.03 mM for the first 400 h, then gradually increased to ~0.1 mM. Potassium concentrations in the effluent of column SW were consistently 0.027 to 0.038 mM, indicating the presence of some K sourced from the soil (Figure S4A in SM). In contrast to the wollastonite columns, very little K was discharged in the mixture columns irrigated with K_3PO_4. The K concentrations were stable at ~0.04 mM throughout the experiment in all MP columns.

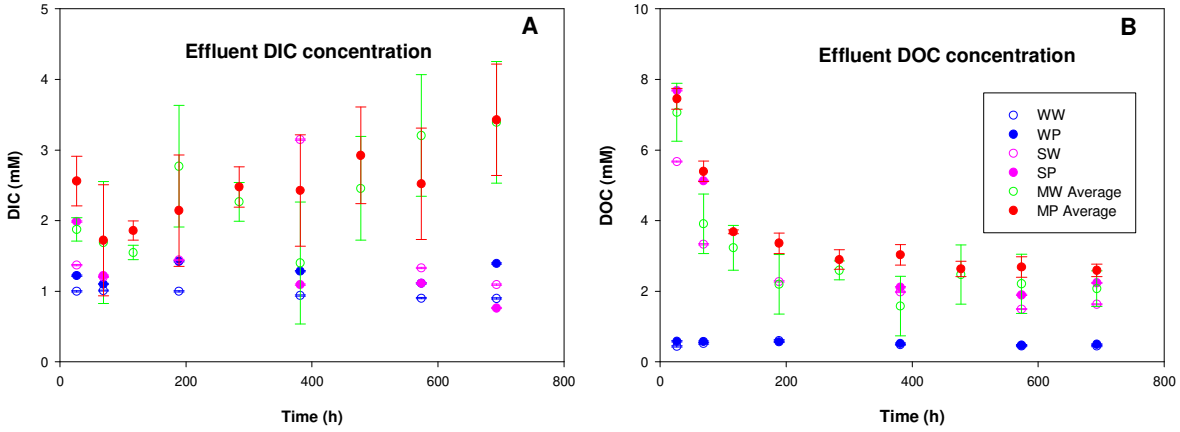

Figure 7: Dissolved inorganic carbon concentrations of column effluent (A) and dissolved organic carbon concentrations of column effluent (B). Mixture column data is presented as an average of three replicate columns. Error bars for non-replicated columns indicate the maximum standard deviation (SD) of triplicate samples (maximum SD was used where only one sample was analyzed for a time point) and error bars for replicated columns indicate the SD of concentrations in samples taken at the same time point for replicate columns. WW (Wollastonite-Water), WP (Wollastonite-P), Soil-Water (SW), Soil-P (SP), MW (Mixture-Water), MP (Mixture-P), where mixture indicates an 8:1 mixture of soil and wollastonite.

In all columns containing soil, DOC concentrations were elevated compared to wollastonite columns, with concentrations of approximately 8 mM at the beginning of the experiments. The DOC in the soil-bearing columns then declined to ~2-3 mM by 200 h, followed by a gradual decline to values between 1.60-2.71 mM by the end of the experiment (Figure 7 B). The trends observed for DOC concentrations were similar for all columns containing soil both with and without P and wollastonite. Dissolved organic carbon was present in the wollastonite columns at low concentrations, remaining stable at 0.40 to 0.61 mM throughout the experiment (Figure 7 B). Dissolved inorganic C concentrations in the fluid samples from the wollastonite and pure soil columns were relatively constant throughout the experiment. Most samples were in the range of 0.75-1.50 mM C in both types of columns, although concentrations in WP were consistently slightly higher than for WW (Figure 7 A). The DIC in effluent from the mixture columns was higher than the wollastonite and pure soil columns and increased throughout the

experimental duration to a maximum of 4.36 mM (Figure 7 A). No substantial differences in DIC concentration were evident between the MW and MP columns. A maximum DIC concentration of 0.18 mM was measured in the influent solution.

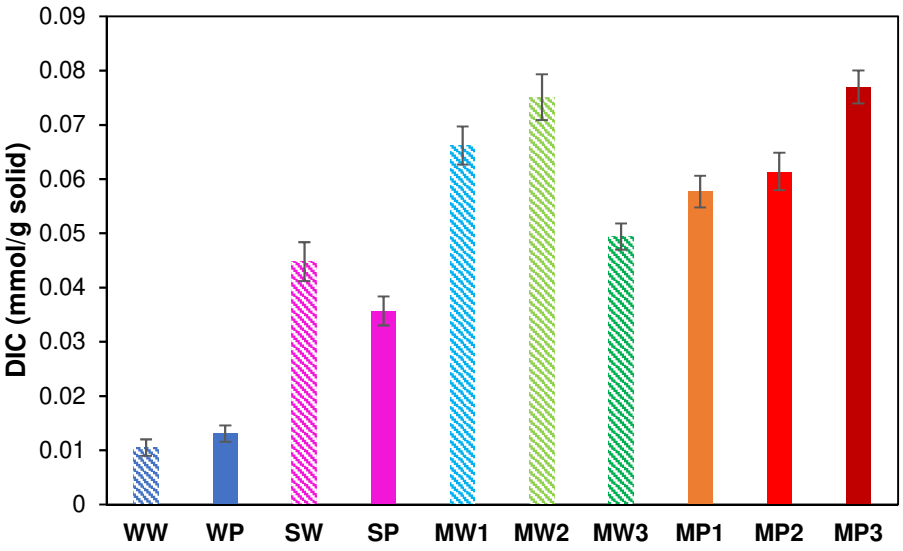

Figure 8. Cumulative dissolved inorganic carbon (DIC) exported from columns normalized to initial total solid mass in each column. Error bars indicate the propagated error for the sum of DIC concentrations and fluid mass. WW (Wollastonite-Water), WP (Wollastonite-P), Soil-Water (SW), Soil-P (SP), MW (Mixture-Water), MP (Mixture-P), where mixture indicates an 8:1 mixture of soil and wollastonite.

The greatest amount of DIC was exported from the mixture columns compared to the wollastonite and soil columns (Figure 8). The maximum amount of DIC exported was from MP 3, with 1.10 mmol total DIC exported over the experimental duration (Figure 8). There were variations in total DIC export between triplicate mixture columns, which ranged from 0.68 to 0.96 mmol and 0.84 to 1.10 mmol in the water and K_3PO_4 columns, respectively. No substantial difference in DIC export was documented between mixture columns irrigated with K_3PO_4 and those irrigated with water (Figure 8). Export of DIC from column WP was 0.002 % greater than column WW, but differences in DIC export between the mixture columns was within measurement uncertainty (Figure 8). Both wollastonite columns exhibited the least DIC export overall (Figure 8). The calculated pCO_2 assuming equilibrium with the measured DIC was significantly greater in the soil and

mixture columns than in the wollastonite columns (Figure S5 in SM). The calculated pCO_2 declined over time in the mixture columns, stabilizing at approximately 2000 ppm by 200 h, yet pCO_2 in the soil and wollastonite columns did not display any clear trend. The calculated pCO_2 in the wollastonite columns was between 24 to 74 ppm throughout the experiment, indicating that the leachate was not at equilibrium with an atmospheric pCO_2 of ~400 ppm. The average concentration of DIC in the influent solution was 0.16 mM. Columns therefore received approximately 0.056 mmol of DIC due to irrigation throughout the experiment. This equates to 16.45, 12.48, 10.14, 12.96, 6.87, and 6.11 % of the DIC discharged from the WW, WP, SW, SP, MW average, and MP average columns respectively.

For the majority of the duration of the experiment, the concentrations of most elements were the same within experimental uncertainty for the mixture-water and mixture-P columns based on the standard deviation between measurements from the triplicate experiments. The implication is that the P-treatment at the applied rate and concentration had no significant impact on wollastonite weathering rates in the wollastonite-soil mixture columns over the month-long experimental duration. The lack of replicates for the wollastonite only columns means that no concrete statistics can be calculated pertaining to the effect of P on wollastonite in the wollastonite only columns. However, there was little difference in effluent concentrations between the wollastonite column receiving the P-treatment and that receiving water, consistent with the lack of impact of P on weathering observed in the mixture columns.

Because the columns received high levels of irrigation, with some columns receiving up to 35% more irrigation relative to their pore volume than others, effluent samples from the wollastonite and soil columns may have experienced dilution relative to the mixture columns. However, the degree of potential dilution and its relevance could not

be robustly quantified for the present experiment. The average loss in column mass between irrigation sessions, which may be considered equivalent to the evaporation that took place between each irrigation, was equal to 4% ± 0.46% of the water content of the columns. Changes in water content and thus water-filled pore volume and evapoconcentration are thus not expected to have substantially affected measured concentrations or the mineral-fluid interface.

3.3 Trends in mineral saturation states

The fluids were undersaturated with respect to wollastonite throughout the experiment in all columns, indicating dissolution of wollastonite was possible throughout the experiment in the bulk fluid (Figure S6 in SM). Calcite was supersaturated in both pure wollastonite columns throughout the entire experimental duration. Column WP was slightly more supersaturated with respect to calcite than column WW ($SI_{calcite}$ = ~0.9 compared to ~0.6). Calcite was consistently undersaturated in both soil columns, indicating antecedent calcite in the soil was favoured to dissolve rather than precipitate. In most of the mixture columns (except MW 1), calcite was undersaturated at the beginning of the experiment, but became supersaturated after 200 h and its degree of supersaturation continually increased throughout the experiment. Magnesium concentrations were only available for the mixture columns and the SI of dolomite displayed a similar trend to that of calcite and remained supersaturated throughout the experiments, with no clear difference between columns receiving water and K_3PO_4 solution. Amorphous silica was undersaturated for the entirety of the experiment in both the wollastonite and soil columns. In all mixture columns, amorphous silica remained near equilibrium for the duration of the experiment, with moderately higher SIs in the MP than the MW column effluent.

555 Hydroxylapatite reached supersaturation in all columns that contained wollastonite
556 and received the K_3PO_4 solution. Hydroxylapatite was supersaturated for the entirety of the
557 experiment in column WP. Quartz was initially supersaturated in the soil columns but
558 became undersaturated by 100 h, where it is initially present. In the mixture columns, quartz
559 was supersaturated at all time points. Polymorphs of SiO_2 (chalcedony, coesite, cristobalite,
560 and tridymite) were indicated to be supersaturated in the wollastonite and mixture columns.
561 However, formation of coesite, cristobalite, and tridymite requires elevated
562 temperature/pressure conditions (Swamy et al., 1994). Although formation of chalcedony
563 has been documented at temperatures < 100 °C, it is typically associated with more elevated
564 temperatures than the experimental temperature in the present study (25 °C) (Heaney,
565 1993).
566

567 **4. Discussion**

568 *4.1. Processes controlling elemental fluxes*

569 Several processes may impact the release of elements during enhanced weathering
570 of wollastonite, including dissolution of wollastonite itself, dissolution of the antecedent
571 minerals in the soil, adsorption and desorption from mineral and organic surfaces, and
572 precipitation of secondary phases. To evaluate the efficacy of wollastonite weathering for
573 CO_2 storage, it is necessary to quantify the extent of weathering of wollastonite and
574 resultant element fluxes (Ca, Si, DIC). The trends in release of elements from the soil and
575 wollastonite columns can shed light on the extent to which elements detected in the mixture
576 column effluent may have originated from the soils themselves, and to what extent the soils
577 impacted the weathering of wollastonite. However, the geochemical conditions evolved
578 differently in the wollastonite and soil end members compared to the mixtures, implying

579 that the soil endmember cannot be treated simply as “background,” with element fluxes
580 subtracted from those from the mixtures.
581 In the wollastonite columns, dissolution of wollastonite was the only source of Si
582 and Ca. Although stoichiometric dissolution of wollastonite results in equivalent moles of
583 Si and Ca being released, the ratio of Si to Ca exported was consistently > 1 for columns
584 WW and WP, respectively. Because amorphous silica was undersaturated in the bulk fluid
585 throughout the experimental duration in the wollastonite columns, and aqueous Si is
586 predominantly present as a neutrally charged species (H_4SiO_4) at the experimental pH, it is
587 likely that Si behaved conservatively in the wollastonite columns. Stoichiometric
588 dissolution of wollastonite is expected over the pH range measured in the experiments
589 (Schott et al., 2012), which implies that Ca was significantly retarded within the
590 wollastonite columns. Retention of Ca in the wollastonite columns could be due to
591 formation of calcite or due to sorption of Ca. Calcite was supersaturated throughout the
592 experimental duration in the wollastonite columns, indicating that calcite formation was
593 possible. Although calcite was not detected by XRD in the wollastonite columns, the SIC
594 content of the upper portion of column WW was observed to increase, suggesting that there
595 was likely some precipitation of calcium carbonate in the column. The increase from 0.025
596 to 0.064 % inorganic carbon in the upper portion of column WW, if applied to the entire
597 column could represent up to 0.13 mmol of Ca incorporated into solids as $CaCO_3$.
598 Precipitation of hydroxylapatite could also incorporate Ca and P in columns receiving P,
599 although no phosphate minerals were detected by XRD or by SEM imaging. The fact that
600 precipitation of calcium carbonate does not account for 100% of the difference in Ca and Si
601 export suggests that sorption of Ca could also have occurred in WW. Wollastonite surfaces
602 are negatively charged at pH > 2.6, favouring cation adsorption (Panday et al., 1986), and
603 cations have been observed to adsorb to wollastonite surfaces at circumneutral pH (Sharma

et al., 1990), comparable to the pH range in the columns of 6.85 to 9.35. Adsorption of Ca to wollastonite surfaces could in part account for its retention in the wollastonite columns. The removal of Ca relative to Si was not observed in the wollastonite dissolution mixed-flow experiments of Schott et al. (2012), but this may be due to the much lower solid:fluid ratio in mixed-flow experiments compared to columns, and the continuous refreshing of inlet solution, compared to the periodic refreshment of the inlet solution in the present study. Although the aqueous P species at the experimental conditions are negatively charged or neutral, P may still form surface complexes with wollastonite, as occurs when $H_2PO_4^{2-}$ promotes the dissolution of wollastonite at pH 2 to 9 (Pokrovsky et al., 2009). The formation of surface complexes could limit the mobility of P in solution in the wollastonite columns. A sorption capacity of 123.31 mg P kg^{-1} wollastonite (Fondu et al., 2010) could potentially capture > 5 mmol P, which exceeds the 1.24 mmol P estimated to be retained within the column. If all P in column MP 2 were removed through precipitation of hydroxylapatite, it would correspond to a mass of 0.623 g, or 4.36% of the dry column mass. This mass would be detectable by XRD, suggesting that sorption rather than precipitation was the dominant process controlling P retardation.

The results of PHREEQC calculations indicate that HCO_3^- was the dominant species at all time points in the wollastonite columns and mixture columns (Figure S7 in SM). If every mole of DIC, which is dominantly HCO_3^-, corresponds to 0.5 moles of wollastonite dissolved (Equation 1), 0.17 and 0.23 millimoles of wollastonite are estimated to have dissolved in columns WW and WP respectively. For column WW, effluent concentrations of Si and Ca indicate 0.42 and 0.16 millimoles of wollastonite dissolution respectively, while Si and Ca concentrations in column WP correspond to 0.31 and 0.18 millimoles of wollastonite dissolution. The difference between wollastonite dissolution predicted by DIC (or alkalinity) and by effluent Si concentrations indicates that alkalinity

may have been retained through SIC or lost by degassing, meaning DIC concentrations do not necessarily represent the true extent of silicate weathering. The lower amount of wollastonite dissolution estimated using Ca is more similar to the DIC method, which could indicate retention of both Ca and C within SIC. However, if the SIC content of the upper portion of column WW is assumed to apply to the entire column, then up to 0.10 millimoles of C are estimated to be contained within SIC. A similar value of 0.13 millimoles of Ca are estimated to be contained in SIC in column WP. For both WW and WP, this estimated Ca removal through SIC formation is not enough to account for all of the difference between Si and Ca release, suggesting sorption of Ca at the mineral surface.

An integrated calculation of Si and Ca release from the soil columns indicates that the soils exported up to 0.101 and 0.052 mmol of Ca and Si, respectively during the experiment. This soil Si and Ca could have originated from the dissolution of Si and Ca-bearing phases in the soils, such as albite and calcite, or from release of Si and Ca ions adsorbed to mineral and organic surfaces. Although Si is present primarily as a neutrally charged complex (excluding organic Si-complexes) under these pH conditions, its potential to adsorb to and desorb from soils (Haynes and Zhou, 2020) and competition with phosphate for adsorption sites has been documented (Lee and Kim, 2007; Obihara and Russell, 1972; Roy et al., 1971). Quartz was undersaturated for the majority of the experiment in the soil columns, indicating it could dissolve and release the observed Si. The SI of albite could not be determined because Al concentrations of the column effluent were not measured. The rapid decline in effluent Si concentrations suggests that aqueous Si was derived primarily from ion desorption and the available exchange sites were quickly exhausted. The only Ca-bearing mineral phases detected by XRD in the soils were minor amounts of calcite and dolomite, and possibly albite if Ca were present in the crystal structure. Calcite was undersaturated throughout the entirety of the experiment in the soil

columns, but the SI of dolomite could not be determined as Mg concentrations were not measured. The decrease in effluent Ca concentrations over time is consistent with desorption of Ca ions from soil surfaces and/or a decreasing amount of dissolution of soil calcite over time. The removal of P in the soil column to below the limit of detection (0.00656 M) and the fact that hydroxylapatite was consistently undersaturated, suggests that P was removed from the solution through adsorption. Notably, it is possible for P to adsorb to clay minerals at neutral to alkaline pH despite negatively charged soil surfaces favouring adsorption of cations (Lee and Kim, 2007; Obihara and Russell, 1972; Roy et al., 1971). Inorganic C fluxes from the soil columns may have been sourced from dissolution of calcite or dolomite, dissolved atmospheric CO_2, or organic C converted to DIC. The much higher pCO_2 in the soil columns compared to atmospheric pCO_2 suggests the DIC was derived primarily from the soils.

Silicon released to solution in the mixture columns may have been derived from the above-described processes documented in the soil columns, in addition to dissolution of wollastonite. Quartz was supersaturated in all mixture columns, thus would not contribute to the Si released. The saturation index of albite could not be determined, so it is unknown to what extent albite contributed to the Si release. However, the dissolution rate constant of albite is > 600-fold lower than wollastonite at the pH conditions of the experiment (Palandri and Kharaka, 2004), so the majority of Si was likely sourced from wollastonite dissolution. Moreover, the Si concentrations in the mixture columns were much higher than in the soil columns. Precipitation of crystalline Si-bearing phases is not expected in the columns over the short timescale of the experiments. Amorphous silica remained close-to-equilibrium throughout most of the experimental duration in the mixture columns, suggesting precipitation of amorphous silica was possible. However, the high Si:Ca ratio relative to stoichiometric wollastonite dissolution suggests significant precipitation of Si is unlikely.

679 Therefore, the main process controlling Si release in the mixture columns is most likely the
680 dissolution of wollastonite.
681 Although initially undersaturated within the mixture columns, the fluid became
682 supersaturated with respect to calcite within approximately 200 h and the calcite saturation
683 index continued to increase throughout the experimental duration. The SIC content of MW
684 1 and MP 1 (other mixture columns were not measured) was observed to increase between
685 the initial and final solids, suggesting calcite may have precipitated. Calcite was therefore
686 likely a more significant sink than source of Ca in the mixture columns. Adsorption to soil
687 surfaces was also likely a sink for Ca within the mixture columns. Similar to what was
688 observed in the wollastonite columns, more Si than Ca was discharged in all mixture
689 columns for at least the first 600 h of the experiment. After 600 h, Si and Ca concentrations
690 began to approach parity. The rising Ca concentrations between 100 h and 400 h followed
691 by stabilization in the mixture columns are consistent with Ca adsorption sites being filled,
692 and thus less available, over time. Adsorption of some of the Ca released through
693 wollastonite dissolution to soils could lead to a lower Ca concentration in outlet fluids
694 compared to Si concentrations. If wollastonite continued to dissolve at a similar rate over
695 time, as adsorption sites became less available the Ca concentration in the effluent would
696 increase and approach the Si concentration. Sorption of a significant portion of the Ca
697 released would necessitate a sufficient cation exchange capacity (CEC) to accommodate the
698 Ca ions. The CEC of a soil can be estimated based on its clay and organic content (Appelo
699 and Postma, 2004):
700 $$CEC\left(\frac{meq}{kg}\right) = 7 \cdot (\%\, clay) + 35 \cdot (\%C) \qquad \textit{Equation 4}$$
701 No clay minerals were identified by XRD in the soils used in the columns.
702 However, the initial soil material contained 29.0 % organic carbon. With this abundance of
703 organic C, a CEC of 1015 meq/kg for the soil is calculated using Equation 4. For an average

mixture column soil mass, there is 12.46 meq of CEC, which equates to an adsorption potential of 6.23 mmol of Ca. This adsorption capacity is approximately 10-times greater than the maximum quantity of Si exported (0.632 mmol), which may provide an indication of the amount of Ca released through stoichiometric dissolution, implying that the exchange capacity was likely in excess of that required to account for the non-stoichiometric Ca and Si release. The increase in Mg concentrations towards the end of the experiment is also consistent with ion exchange sites becoming filled over time, in addition to the observed increase in P and K concentration in some column fluids. Although a small increase in SIC was observed in columns MW 1 and MP 1, it is insufficient to account for the gap between Ca and Si concentrations, except for the anomalously high SIC increase observed in column MW 1. Sorption is thus sufficient to explain all Ca retardation within the mixture columns and was likely a more significant sink than precipitation of Ca-bearing minerals over the experimental timescales. The lesser export of Ca than DIC within the wollastonite and mixture columns is consistent with sorption being an important mechanism for the retention of Ca (Figure 9). However, the lower Ca and DIC export relative to stoichiometric wollastonite weathering based on Si concentrations suggests removal of DIC by precipitation may also occur and contribute to Ca removal from solution (Figure 9).

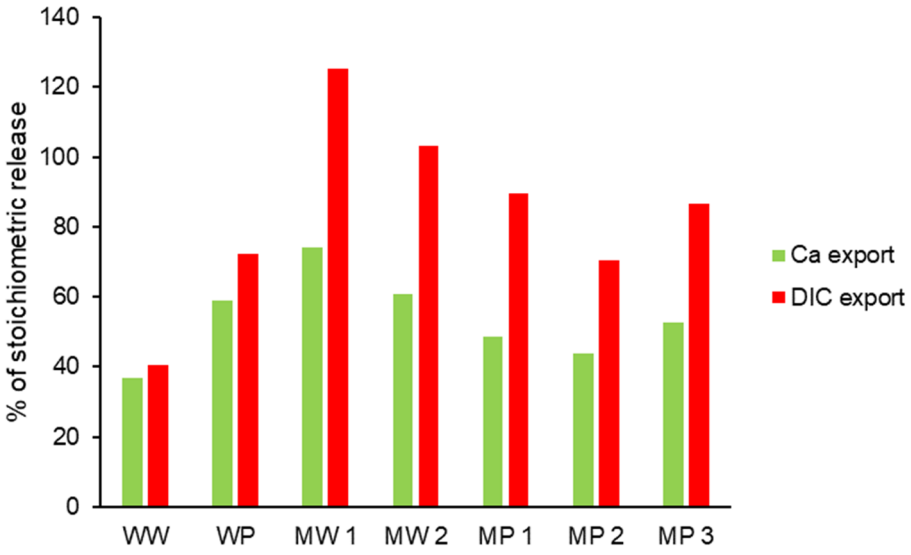

Figure 9. Export of Ca and DIC as a percent of stoichiometric release from wollastonite. Stoichiometric release was calculated relative to Si concentrations assuming reaction stoichiometry of Equation 1. Wollastonite-Water (WW), Wollastonite-P (WP), Mixture-Wollastonite (MW), Mixture-P (MP) where Mixture indicates an 8:1 mixture of soil and wollastonite.

Unlike the wollastonite or soil columns, all mixture columns displayed an increase in effluent DIC concentrations over time. Dissolution of calcite could only be a source of DIC during the first 200 h of the experiment because it became supersaturated in bulk solution after this time point. Interactions between microbially-generated CO_2 and wollastonite may provide an explanation for the increasing DIC concentrations over time observed in the mixture columns. Heterotrophic bacteria are known to metabolize organic carbon and produce CO_2 as waste through aerobic respiration. The trend of increasing DIC concentration was not observed in either the wollastonite or soil columns, implying it resulted from an interaction between the soils and wollastonite. If the increase in DIC concentration was not attributable to an increase in wollastonite dissolution and thus alkalinity generation over time, then it could be due to incomplete flushing of DIC during irrigation and residual build-up of DIC or possibly due to an increase in microbial activity over time. However, it was only in the mixture columns that an increase in DIC over time

742 was observed. Based on this distinction, it appears that the presence of wollastonite
743 promoted the conversion of soil CO_2 to DIC, perhaps mediated by microbial activity.
744 Enhanced microbial activity compared to soil columns could be due to contribution of
745 nutrients from wollastonite. Notably, due to soil CO_2 production resulting in a pCO_2 in
746 excess of atmospheric pCO_2, the concentration gradient would not have favoured CO_2
747 ingress from the atmosphere. However, measurements of influent DIC concentration
748 indicate that 6 to 7 % of the DIC measured in mixture column effluent was of atmospheric
749 origin, introduced through irrigation.

750 The different processes operating in the mixture columns as compared to the
751 wollastonite columns demonstrate that dissolution behavior and rates of pure mineral
752 phases cannot be directly applied to soil amendments. Mixture columns released
753 comparable amounts of Ca and Si as wollastonite columns despite approximately 22 times
754 lower mass of wollastonite, indicating that the wollastonite weathering rate was
755 significantly greater in the mixture columns. The differences in elemental fluxes between
756 the mixture columns and the wollastonite and soil only columns illustrate that the influence
757 of mineral-soil interactions is not simply additive. Minerals that tend to dissolve in soils
758 may become oversaturated due to the presence of mineral amendments, meaning their
759 contribution to element fluxes would be limited. In soil-mineral mixtures, sorption may
760 change from a source to a sink for cations such as Ca, and interactions between microbially-
761 produced CO_2 and mineral amendments may significantly impact fluxes of DIC. The
762 processes controlling CO_2 storage are thus not wholly represented by either mineral or soil
763 endmembers. The emergence of unique processes in mineral-amended soils necessitates
764 site-specific characterization of mineral-soil mixtures and complicates prediction of
765 weathering rates and CO_2 capture.
766

767 *4.2. Wollastonite Weathering Rates*

768 The wollastonite and mixture columns approached steady-state conditions based on
769 pH and release of Ca and Si within 600 h. Bulk dissolution rates of wollastonite can be
770 estimated based on the concentrations of Si. After 600 h, concentrations of Si in the columns
771 irrigated with water were 0.88-1.19 mM for the wollastonite column and 1.04-1.38 mM for
772 the mixture columns, respectively. After 600 h in the columns irrigated with K_3PO_4, Si
773 concentrations were 0.56-0.71 mM for the wollastonite column and 1.09-1.43 mM for the
774 mixture columns. Because Si in the mixture column effluent primarily originates from
775 dissolution of wollastonite, this suggests that bulk wollastonite dissolution rates in the
776 mixture columns receiving K_3PO_4 were up to twice the dissolution rate of wollastonite in the
777 wollastonite column receiving K_3PO_4, and dissolution rates of wollastonite columns receiving
778 water were within the range of mixture columns receiving water. However, the 22-times
779 greater mass of wollastonite in the wollastonite column compared to mixture columns implies
780 the surface or mass-normalized dissolution rate of wollastonite was in fact ~22-times greater
781 in mixture columns.

782 Previous experiments have shown that $H_2PO_4^-$ enhances the rate of wollastonite
783 dissolution (Pokrovsky et al., 2009), however, no consistent difference in wollastonite
784 weathering rate in columns irrigated with K_3PO_4 was evident in any of the columns in the
785 present study. Release of Si was more rapid in the first 400 h of the experiment in the mixture
786 columns receiving K_3PO_4 compared to the mixture columns receiving water. However, this
787 early Si release may be attributable to lower initial pH in the MP columns compared to the
788 MW columns. The only evidence of enhanced dissolution in column WP compared to WW
789 was the slightly higher pH and greater Ca concentration in column WP than WW. However,
790 Si release was greater in the WW column, inconsistent with a P- enhanced wollastonite
791 dissolution rate. Similarly, despite a ~38% higher total Si export (0.16 mmol) for the average

792 of the triplicate mixture columns receiving K_3PO_4 compared to those receiving water, Ca
793 release was approximately equal. Although Ca-bearing precipitates may have formed in the
794 mixture columns receiving K_3PO_4, evidence of their presence was not observed. The similar
795 concentrations of elements measured for the MW and MP columns, within experimental
796 uncertainty, suggests that the P treatment did not significantly enhance the dissolution of
797 wollastonite within the mixture columns. Although differences in concentration of Si, Ca, and
798 DIC for the wollastonite columns with and without P supplied are outside of analytical
799 uncertainty, it cannot be concluded whether these small differences were the result of P, due
800 to the lack of replicate experiments for these conditions. However, because the mixture
801 columns display no substantial impact of P on weathering rate, coupled with the low P
802 concentrations relative to those required to significantly accelerate wollastonite dissolution
803 (Pokrovsky et al., 2009), it is unlikely that P significantly affected weathering rates in the
804 wollastonite columns.

805 The lack of impact of P on wollastonite weathering is likely due to the rapid removal
806 of P from solution in all columns, limiting its capacity to enhance weathering rates (Figure 6).
807 Moreover, the speciation of P in solution is likely to govern its influence on dissolution rate,
808 as not all dissolved P species enhance dissolution rates depending on the type of surface
809 complex that forms (Pokrovsky et al. (2009). Pokrovsky et al. (2009) documented that
810 $H_2PO_4^-$ enhanced the dissolution of wollastonite but suggested that other dissolved P species
811 may not equally enhance, or could inhibit, dissolution based on the interactions that have
812 been documented with brucite and goethite. Surface complexes that bond to only one metal
813 are predicted to promote wollastonite dissolution to a far greater extent than bi- or multi-
814 dentate complexes with more than one nucleus (Pokrovsky et al., 2009). The species $H_2PO_4^-$
815 forms monodentate surface complexes that promote wollastonite dissolution. Speciation
816 calculations indicate that despite declining concentrations at elevated pH, approximately 16%

817 of P would still have been present as $H_2PO_4^-$ in the mixture columns receiving K_3PO_4,
818 potentially enhancing the dissolution rate of wollastonite (Figure S8 in SM). In the
819 wollastonite columns, in which pH was consistently > 9, less than 2% of the P would be
820 present as $H_2PO_4^-$, limiting its impact on rate (Figure S8 in SM). The pH of soil pore water
821 will therefore play a strong role in dictating the effect of dissolved P on wollastonite
822 dissolution in enhanced weathering scenarios through its impact on both aqueous speciation
823 and removal from solution by adsorption. The mixture columns showed that P removal
824 during ERW may occur by adsorption, however, over longer timescales P concentrations
825 could increase towards the influent concentrations due to saturation of adsorption sites. It is
826 possible that over longer timescales, P addition may exert a greater impact on weathering
827 rates. Moreover, at higher concentrations of P added, the impact on weathering may have
828 been greater. The impact of P on silicate weathering during ERW therefore merits further
829 study over a broader range of conditions and over longer timescales.
830 The median pH of the wollastonite columns exceeds the mixture column pH by as
831 much as 1.47 pH units. The lower pH in the mixture columns is partially attributable to less
832 reactive surface area of wollastonite in the mixture columns compared to the wollastonite
833 columns, and the higher soil pCO_2. The wollastonite columns had a much higher
834 wollastonite-fluid ratio, with a greater potential for pH increase through wollastonite-fluid
835 interaction, but this higher pH would engender a reduction in wollastonite dissolution rate. It
836 is feasible that microbial activity also played a role in promoting dissolution in the mixture
837 columns. The soils used in this experiment were rich in organic matter, with an organic
838 carbon content of 29.0% prior to reaction. In addition to organic acids, carbon dioxide
839 released by bacteria dissolves in porewaters and forms carbonic acid, leading to lower
840 porewater pH (Eq. 5):
841 $$CO_2 + H_2O \leftrightarrow H_2CO_3 \leftrightarrow HCO_3^- + H^+ \leftrightarrow CO_3^{2-} + 2H^+$$ *Equation 5*

The rate and mechanism of the dissolution of wollastonite depend strongly upon the pH of the fluid (Schott et al., 2012). When pH ≥ 4.8, as it was in all the present experiments, the dissolution rate can be described by (Eq. 6; Schott et al., 2012):

$$r_{+,Si,pH\geq 5} = 10^{-11.41} a_{H^+}^{0.18} \qquad \textit{Equation 6}$$

Where, $r_{+, Si}$ is the dissolution rate (mol/cm^2/s) expressed for release of Si, and a_{H+} is the activity of H^+ in solution. Calculated bulk dissolution rates (i.e., for the total surface area of wollastonite in each column) based on the median pH value and Equation 6 for each wollastonite-containing column are provided in Table 4. Due to the lower pH, the surface area-normalized mixture column dissolution rates for the average of the triplicate columns is approximately 38 and 35 times greater in the MW and MP columns, respectively, than in the wollastonite-water column due to the difference in pH between columns alone. Thus, pH-dependence of the dissolution rate can largely account for the higher dissolution rate in the mixture compared to the wollastonite columns.

Table 4. Calculated wollastonite dissolution rate based on median column pH and measured elemental release rates

Column[a]	pH[b]	SA[c] (cm^2)	pH-dependent Dissolution Rate (mol/cm^2/s)[d]	pH-dependent Rate/WW[e]	Measured Ca Rate/WW[e]	Measured Si Rate/WW[e]
WW	9.17	46607	1.87E-18	1.0	1.0	1.0
WP	9.23	49165	1.73E-18	0.93	1.1	0.6
MW 1	7.87	2084	7.15E-17	38.3	50.9	20.1
MW 2	7.93	2022	7.19E-17	38.5	60.6	32.8
MW 3	7.86	2181	6.86E-17	36.8	50.5	26.4
MP 1	7.87	2292	6.50E-17	34.8	40.5	20.2
MP 2	7.76	2255	6.92E-17	37.1	52.1	32.2
MP 3	8.07	2251	6.09E-17	32.7	64.9	31.2

[a]Wollastonite-Water (WW), Wollastonite-P (WP), Mixture-Water (MW), Mixture-P (MP) where mixture indicates an 8:1 mixture of soil and wollastonite.
[b]pH values represent the median pH of effluent samples for each column.
[c]SA represents the total surface area of wollastonite in the column based on BET analysis.
[d]pH-dependent dissolution rate was calculated based on the median pH for each column and surface area (SA) using the rate law of Schott et al. (2012).
[e]Rates are normalized to the calculated pH-dependent WW or measured WW value. Measured Ca Rate/WW and Measured Si Rate/WW are based on the average rate of Ca and Si discharge from each column within the last 400 h of the experiments, relative to the measured rates in WW during the same period.

867 Dissolved CO_2 can also promote wollastonite dissolution through formation of HCO_3^-
868 ligands. Under acidic conditions (pH ~4), the concentration of CO_2 is insignificant to the
869 overall dissolution rate, but at circumneutral pH, HCO_3^- was shown to slightly increase the
870 dissolution rate of wollastonite (Golubev et al., 2005; Pokrovsky et al., 2009). However, the
871 concentrations of HCO_3^- in the present experiment were notably lower than required to
872 double the dissolution rate of wollastonite, at < 5mM compared to 10 mM (Golubev et al.,
873 2005). Several organic ligands have also been shown to enhance the dissolution of
874 wollastonite (Pokrovsky et al., 2009). Maximum total DOC concentrations of ~ 8 mM were
875 in excess of the concentrations of EDTA, catechol, gallic acid, and 8-hydroxychinolin
876 necessary to triple the dissolution rate of wollastonite at neutral pH (Pokrovsky et al., 2009).
877 The impact of these additional ligands could account for some of the gap between the
878 theoretical dissolution rates predicted by the pH-dependent rate law (Schott et al., 2012) and
879 the measured release rates of Ca and Si in the mixture columns.

880 *4.3. Quantification of CO_2 Storage by Wollastonite Weathering*

881 There are numerous geochemical processes operating in the columns that could
882 influence the cycling of carbon. Some of these processes would result in carbon storage,
883 some in carbon release, and some are net neutral with respect to the carbon balance. Before
884 quantifying carbon storage within the columns, these reactions, and their effects on the
885 fluxes of C from various sources must be defined. The degradation of soil organic matter
886 and DOC can result in release of CO_2 to the atmosphere, which is consistent with the
887 greater than atmospheric pCO_2 calculated in the soil and mixture columns (Figure S5 in
888 SM). Conversely, the weathering of wollastonite is the primary mechanism by which
889 atmospheric CO_2 is sequestered in the columns. At circumneutral pH, wollastonite
890 weathering proceeds according to Equation 1 and brings CO_2 into solution as dissolved
891 inorganic carbon. If this CO_2 is sourced from the atmosphere, the result of wollastonite

dissolution is net removal of CO_2 from the atmosphere. On the other hand, if the CO_2 driving wollastonite weathering is from the oxidation of soil organic matter, wollastonite weathering may instead represent mitigated CO_2 emissions of soil-generated CO_2 rather than net removal of modern atmospheric CO_2. The effect of wollastonite weathering in the latter case is to reduce the flux of CO_2 to the atmosphere from the soils. Similarly, formation of solid carbonate from DIC would result in modern CO_2 removal or avoided CO_2 emissions if the CO_2 source were the atmosphere or soil generated CO_2, respectively. Dissolution of antecedent carbonate in the soil removes or avoids CO_2 in the same way as wollastonite dissolution (Equation 7),

$$CaCO_3 + CO_2 + H_2O \leftrightarrow Ca^{2+} + 2HCO_3^- \qquad \textit{Equation 7}$$

but precipitation of SIC from carbonate dissolution results in no net loss or gain of CO_2. In this study, CO_2 storage is considered to encompass both formation of carbonates and eventual CO_2 storage in the oceans as alkalinity. Thus, in the wollastonite columns, DIC and SIC represent net modern atmospheric CO_2 storage, as the atmosphere is the only DIC source. In contrast, the high pCO_2 in the mixture columns suggests most CO_2 in the mixture columns was derived from soils rather than directly the atmosphere. Measurement of DIC concentrations in the irrigation water indicates that atmospheric CO_2 introduced through irrigation water comprised approximately 6 to 7% of DIC detected in mixture column effluent. Although carbon respired by microbes ultimately originates from the atmosphere, the degree of decomposition of the soil, and therefore the timescale of carbon cycling cannot be determined in the present study. The extent to which the wollastonite mineral amendment affected different carbon pools is unknown. For the purposes of this study, a distinction is therefore made between modern CO_2 directly removed from the atmosphere through ERW, representing negative emissions, and fluxes of soil-generated CO_2 to the atmosphere that have been mitigated as a result of ERW, though both represent CO_2 storage.

In the soil columns, calcite remained undersaturated and may have contributed to the DIC flux in addition to organic C degradation, however in the mixture columns, calcite and dolomite were supersaturated for the majority of the experiment, indicating they were unlikely to dissolve substantially and contribute to the DIC flux (Figure S6 in SM). Thus, the main CO_2 source for DIC in the mixture columns is likely degradation of organic C. The higher pH in the mixture columns compared to the soil columns due to wollastonite dissolution would encourage lower CO_2 loss to the atmosphere due to the greater solubility of CO_2 at higher pH.

Because of the complex set of geochemical interactions impacting DIC, the efficiency of CO_2 removal by weathering is often determined based on cation or Si fluxes (Gaillardet et al., 1999; Kelland et al., 2020; Peters et al., 2004). Calcium concentrations are unreliable tracers of the extent of wollastonite weathering in the present experiments due to adsorption (and possible precipitation) processes. Solid and fluid inorganic carbon are also unreliable indicators of wollastonite weathering within the mixture columns in the present study due to the presence of SIC in soils and the generation of DIC through processes other than wollastonite weathering. Silicon export directly provides a weathering rate that can be related to the CO_2 removal rate though Equation 1, but the possibility for subsequent fluid-soil interactions such as sorption and precipitation creates uncertainty in the mass balance. Despite this limitation, effluent Si concentrations were considered the most precise tracer of wollastonite weathering of those measured in the column experiments. The CO_2 removal rate in the column experiments was therefore calculated using the total Si flux as follows:

$$R_{CR} = \frac{2 \cdot M_{Si,total} \cdot m_{CO_2}}{(m_{wol} \cdot t_{exp})} \qquad \textit{Equation 8}$$

Where R_{CR} is the CO_2 removal rate in kg CO_2 t amendment^{-1} yr^{-1}, $M_{Si,\ total}$ is the total moles of Si exported from the column (multiplied by 2 as each mole of Si is balanced by 2 moles of HCO_3^- per Equation 1), m_{CO_2} is the molar mass of carbon dioxide (kg/mol), m_{wol} is the

mass of wollatonite in the column (t), and t_{exp} is the duration of the experiment (yr). Similar equations were used to calculate CO_2 removal rates based on total fluxes of Ca and DIC, for comparison of different approaches of CO_2 removal calculation (Table S2 in SM).

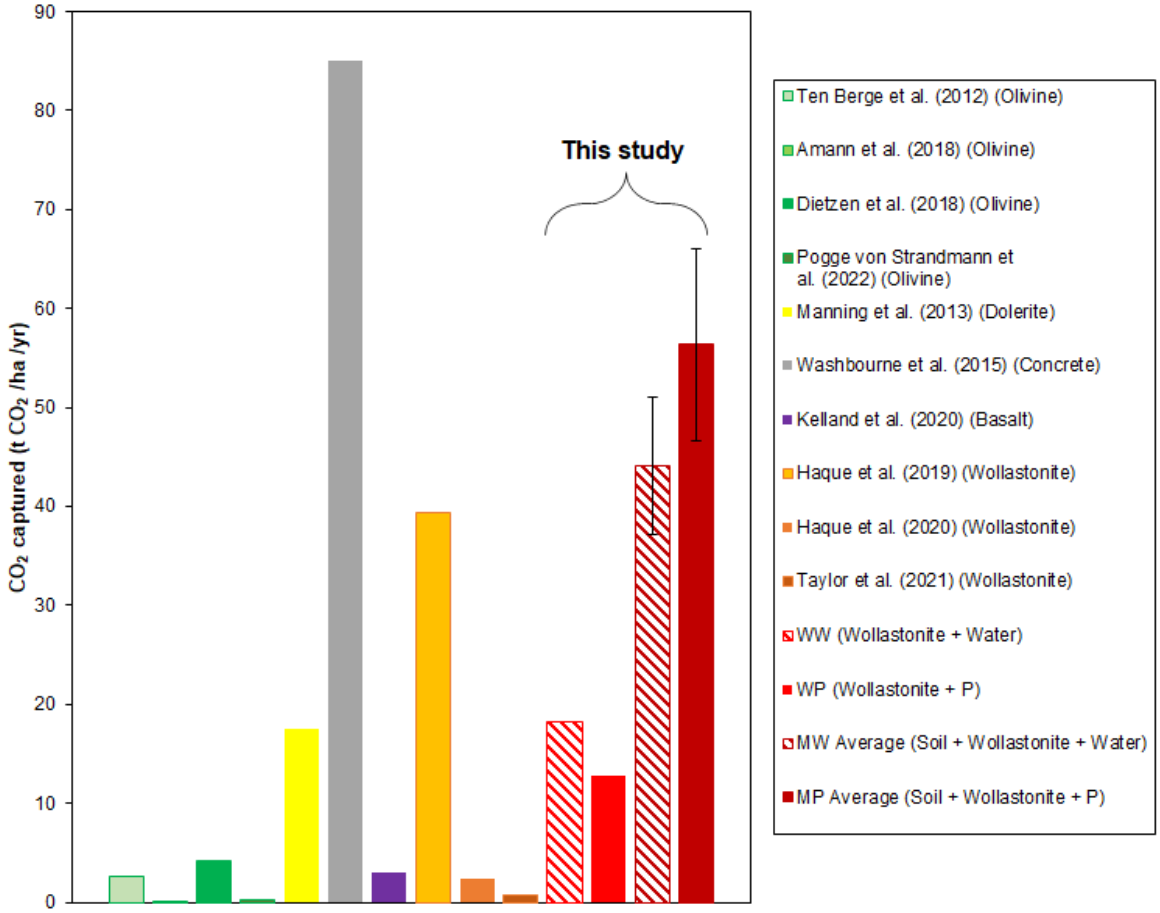

Figure 10. Comparison of CO_2 storage rate in enhanced rock weathering studies. WW (Wollastonite-Water), WP (Wollastonite-P), MW (Mixture-Water), MP (Mixture-P), where mixture indicates an 8:1 mixture of soil and wollastonite. Averages of triplicate MW and triplicate MP columns were used for this study, with error bars indicating standard deviation of the average.

The total mass of CO_2 stored in each column was extrapolated to 1 ha of land area (Table 5, Figure 10) for ease of comparison with previous studies. Manning et al. (2013) documented an SIC accumulation of 17.6 t CO_2 ha^{-1} yr^{-1} with a blend of compost and basalt/dolerite quarry fines, but mesocosm experiments with dunite amended soils captured much less, with an estimated 0.05 t CO_2 ha^{-1} yr^{-1} as DIC (Amann et al., 2020). Other olivine experiments produced upper estimates of 2.69 t CO_2 ha^{-1} yr^{-1} (Ten Berge et al., 2012), 4.16 t

CO_2 ha^{-1} yr^{-1} (Dietzen et al., 2018), and 0.3 t CO_2 ha^{-1} yr^{-1} (Pogge von Strandmann et al., 2022), and basalt mesocosms capturing an estimated 3.01 t CO_2 ha^{-1} yr^{-1} (Kelland et al., 2020). At the higher end of carbon storage rates, Washbourne et al. (2015) showed that weathering of urban soils with a high waste concrete content resulted in capture of 85 t CO_2 ha^{-1} yr^{-1} as SIC (Washbourne et al., 2015). An upper estimate of CO_2 removal rate by wollastonite amendment in the Hubbard Brooke watershed was 0.77 t CO_2 ha^{-1} yr^{-1} (Taylor et al., 2021). Laboratory (Haque et al., 2019) and field (Haque et al., 2020) experiments with wollastonite amended soils and crops produced strikingly different estimates of CO_2 storage with 39.3 t CO_2 ha^{-1} yr^{-1} and 0.28 to 2.4 t CO_2 ha^{-1} yr^{-1}, respectively, with the difference possibly due to lower wollastonite loading in the field study.

The CO_2 removal rates in this study were greater than those documented in many previous experimental ERW studies(Table 4; Amann et al., 2020; Dietzen et al., 2018;Taylor et al., 2021 ; Kelland et al., 2020; Manning et al., 2013; Pogge von Strandmann et al., 2022; Ten Berge et al., 2012). The average CO_2 removal rate in the mixture columns of 50 t CO_2 ha^{-1} yr^{-1} is only exceeded by artificial concrete soils (Washbourne et al., 2015), and is of similar order of magnitude to the pot experiments by Haque et al. (2019) in which plants contributed to wollastonite weathering. However, CO_2 removal rates for the present study when normalized to material loading were closer to other studies and exceeded by those of Dietzen et al. (2018), Haque et al. (2019), and Haque et al. (2020) (Table 5). The material loading normalized CO_2 removal rate for the present study is of similar magnitude to that reported by Taylor et al. (2021) for which wollastonite was applied at the watershed scale. For the present study, if assuming a 1 C: 1 Ca: 1 Si ratio with carbonate precipitation being the primary CO_2 sink rather than DIC, then CO_2 removal rates of 9.1 and 6.4 t CO_2 ha^{-1} yr^{-1} are calculated for columns WW and WP

982 respectively, and 22 and 28 t C ha^{-1} yr^{-1} for the MW and MP columns, respectively (Figure

983 S9).

Table 5. Comparison of CO_2 removal rate in enhanced rock weathering studies

Study	Material	Study Scale	Plant Presence	Material Loading (t /ha)	CO_2 Capture Metric	kg CO_2 /t amendment /yr	t CO_2 /ha /yr
Ten Berge et al. (2012)	Olivine	Pot	Yes	204	Mg Balance	132	2.69
Manning et al. (2013)	Dolerite	Field	Yes	Not stated	SIC	N/A	17.6
Washbourne et al. (2015)	Concrete	Field	No	Not stated	SIC	N/A	85
Amann et al. (2018)	Olivine	Mesocosm	Yes	220	Mg Balance	2.23	0.05
Dietzen et al. (2018)	Olivine	Column	No	50	Mg Balance	832	4.16
Haque et al. (2019)	Wollastonite	Pot	Yes	221	SIC	1778	39.3
Haque et al. (2020)	Wollastonite	Field	Yes	1.25-5.0	SIC	224-4800	0.28-2.4
Kelland et al. (2020)	Basalt	Mesocosm	Yes	100	Mg Balance	30.1	3.01
Taylor et al. (2021)	Wollastonite	Watershed	Yes	3.44	Ca Balance	223	0.77
Pogge von Strandmann et al. (2022)	Olivine	Column	No	127	Mg Balance	2.4	0.30
Wollastonite-Water[a]	Wollastonite	Column	No	1989	Si, Ca, HCO_3^-	3.36-9.13[b]	6.67-18.2[b]
Wollastonite-P[a]	Wollastonite	Column	No	1989	Si, Ca, HCO_3^-	3.75-6.39[b]	7.46-12.7[b]
Mixture-Wollastonite 1[a]	Wollastonite	Column	No	221	Si, Ca, HCO_3^-	126-211[b]	27.7-46.6[b]
Mixture-Wollastonite 2[a]	Wollastonite	Column	No	221	Si, Ca, HCO_3^-	141-239[b]	31.1-52.9[b]
Mixture-Wollastonite-3[a]	Wollastonite	Column	No	221	Si, Ca, HCO_3^-	111-199[b]	24.5-43.9[b]
Mixture-P 1[a]	Wollastonite	Column	No	221	Si, Ca, HCO_3^-	99.3-205[b]	21.9-45.2[b]
Mixture-P 2[a]	Wollastonite	Column	No	221	Si, Ca, HCO_3^-	122-278[b]	26.8-61.4[b]
Mixture-P 3[a]	Wollastonite	Column	No	221	Si, Ca, HCO_3^-	149-283[b]	32.8-62.4[b]

[a]this study

[b]range of CO_2 removal rate calculated using either Si, Ca, or HCO_3^- concentrations

Although the present study indicates a higher CO_2 capture rate on a per area basis than in previous studies, much of the discrepancy can be eliminated by normalizing to the material loading rate. Other factors that may have increased the CO_2 capture rate in the present study beyond what might be expected in field-scale ERW settings include the frequent irrigation and large volume of water used relative to the mass of soil, the purity of the wollastonite amendment, and the experimental length. Porewater content and residence time strongly influence weathering rates and CO_2 uptake from the atmosphere; thus, the irrigation rate could significantly influence CO_2 storage rates (Andrews and Taylor, 2019; Cipolla et al., 2021; Harrison et al., 2015; Harrison et al., 2016). Soil moisture correlates strongly to enhanced weathering of silicate soil amendments due to the increase in accessible reactive surface area of minerals (Cipolla et al., 2021). Columns in the present experiment received approximately 15,900 mm yr^{-1} of irrigation, substantially greater than the 1400 mm average annual precipitation of the Hubbard Brooke Experimental Forest(Taylor et al., 2021). The use of pure wollastonite in the present experiment may have resulted in greater CO_2 capture rates than application of bulk silicate rock. Furthermore, the shorter experimental length could influence the CO_2 removal rate, as wollastonite dissolution rates may slow over time, causing a lower time-averaged rate over longer periods compared to the approximately 700 h of the present experiment.

4.4. Implications for ERW

The overall rates of CO_2 removal for the average of the triplicate mixture columns receiving H_2O and K_3PO_4 were 200 ± 31 kg CO_2 t $amendment^{-1}$ yr^{-1} and 255 ± 44 kg CO_2 t $amendment^{-1}$ yr^{-1}, respectively, overlapping within uncertainty. The addition of P had little influence on the net dissolution of wollastonite in the experiments, largely due to the removal of P from solution by adsorption to mineral and organic surfaces. In soils with

lower cation exchange capacity, or over a longer time and/or higher added P concentrations, the removal of P by adsorption may become less significant, but precipitation as Ca-phosphate phases may occur. No evidence of phosphate mineral precipitation was found in any of the experiments suggesting it was not a major P sink compared to adsorption; however, this may not be the case over longer timescales in the field. In addition, pH changes from the dissolution of wollastonite or other geochemical processes may limit the effectiveness of P for enhancing the dissolution of wollastonite due to alteration of aqueous speciation. In field settings, where P may be taken up by plants or consumed by microbes, its availability in solution to enhance dissolution may be further limited. With so many factors that can reduce the impact of aqueous P on the dissolution of wollastonite, the most significant way in which the application of P-bearing fertilizers is likely to support enhanced weathering is by promoting plant growth. Plants enhance wollastonite dissolution in soils (Haque et al., 2019) and are themselves a carbon sink. The greatest CO_2 capture in a field-scale trial of wollastonite soil amendment was observed in a field that received a P-bearing fertilizer (Haque et al., 2020). However, the nature of interactions between plants, mineral amendments, and fertilizers has not been fully resolved (Mkhonza et al., 2020; Jariwala et al,. 2022; Jakobsen, 1979). Direct interactions between minerals and P-fertilizers are less likely to represent a significant factor in governing CO_2 removal rates.

The physical and chemical properties of soils used in ERW may have crucial implications regarding the dissolution of any mineral soil treatment and resulting element release trends, which cannot be predicted based on dissolution rates and behaviour of pure mineral phases. Our experiments demonstrate that even in fairly simple systems with a pure mineral amendment in soil without plant growth, the complex and coupled interactions between living and abiotic soil components and rock amendments substantially complicate the quantification of CO_2 capture. Differences in surface-area normalized weathering rates

between the wollastonite and mixture columns reveal that the behaviour of pure minerals or background soils do not adequately reflect the conditions of a mineral-soil mixture; elemental releases from individual components are not simply additive. Crucially, because the pH was lower in the mixture columns, more wollastonite dissolved and therefore, more CO_2 was captured or retained than with wollastonite alone. These lower pH values may have resulted from the lower wollastonite:fluid ratio, or from the release of CO_2 from soils due to microbial activity, promoted by the high organic content of the soils. This soil CO_2 was also likely key to the increasing DIC concentrations over time in the mixture columns, but it only became apparent in the presence of wollastonite, not in the soil columns.

Silicon concentrations exceeding those of Ca are atypical in the case of wollastonite dissolution, which is generally stoichiometric at the experimental pH conditions (Schott et al., 2012), yet Si concentrations in excess of Ca concentrations were observed in both mixture and wollastonite columns (Figure 5). However, an increase in Ca concentrations over time was observed only in mixture columns as it most likely resulted from reduced exchange site availability for Ca over time. Calcite went from undersaturated to oversaturated in the mixture columns, potentially resulting in carbonate mineral formation. This stands in contrast to the wollastonite columns, in which less dissolution of wollastonite occurred, but calcite was supersaturated throughout the experiment. Similarly, several soil mineral constituents were undersaturated in the soil columns but were supersaturated in the mixture columns. For example, despite being undersaturated in the soil columns, quartz and calcite were oversaturated in the mixture columns (>200 h). This underscores the fact that elemental release from soils themselves may differ when treated with a soil amendment. The implication is that the presence of soil amendments substantially alters weathering of pre-existing soil minerals. The different trends in DIC for the mixture columns compared to both the wollastonite or soil columns also highlight the importance of evaluating soil

1062 treatments within the soils to be amended. Elements released from the soil amendment (Ca
1063 and Si in this case), as well as DIC and SIC are key indicators of ERW and CO_2 capture.
1064 The importance of considering the effects of soils is supported by complications observed
1065 in previous enhanced weathering experiments (Amann et al., 2020). In a mesocosm
1066 experiment in which soils were amended with dunite, calculated CO_2 consumption by
1067 weathering was up to three orders of magnitude lower than in similar studies (Amann et al.,
1068 2020). The calculation was based on effluent Mg concentrations, which were speculated to
1069 have been retarded by processes such as adsorption, mineralization, uptake by plants, and
1070 preferential flow (Amann et al., 2020). The present study, along with the previous study of
1071 Amann et al. (2020), demonstrate the potential for soils to complicate estimates of CO_2
1072 capture and nutrient release in ERW scenarios. To account for the influence of soils in
1073 evaluations of field-deployed ERW, site-specific characterization of soil-mineral mixtures
1074 is necessary, such as characterizing organic carbon and clay content, mineralogical
1075 composition, and sorption capacity. Evaluation of the microbial populations in soils would
1076 also be valuable, as microbe-soil and microbe-mineral interactions are strong controls on
1077 the evolution of the fluid composition and CO_2 stored. In future field experiments or large-
1078 scale deployment of ERW, it is vital to consider the contribution of soils to elemental trends
1079 observed, as well as how that contribution may be influenced through interactions with
1080 additives. Reactive transport modeling, at both the laboratory and field scale, is important to
1081 define pathways of elemental transport and transformation. For example, the watershed-
1082 scale modeling of Hayder et al. (2019) suggests that interactions between wollastonite and
1083 P may be important not only for CO_2 capture but also for remediation of agricultural
1084 pollution.
1085

5. Conclusion

The capacity of dissolved P to accelerate the dissolution of wollastonite was severely limited by its rapid removal from solution in all columns. This removal was driven by adsorption of P to mineral and organic surfaces and the change in speciation due to the pH increase caused by wollastonite dissolution. These mitigating factors indicate that the capacity of P to accelerate wollastonite dissolution was limited, leading to little impact of added P on observed wollastonite weathering rate.The high pCO_2 of soils suggests that the majority of CO_2 present in the soil/mixture columns, and the majority of CO_2 stored in those columns was released through degradation of organic matter and represents a flux of carbon from soil to the atmosphere that was mitigated, rather than direct removal of modern atmospheric CO_2. Material loading normalized rates of silicate weathering in the mixture columns were similar to those in previous ERW studies, suggesting comparable CO_2 capture/retention to wollastonite application at the watershed scale (Taylor et al., 2021). Possible factors contributing to differences in weathering rate with previous studies include greater mineral loading and irrigation, the use of a more reactive amendment, and a shorter experimental duration. The substantially greater wollastonite dissolution and CO_2 capture in the mixture columns than with wollastonite alone demonstrate that soils exert an important impact on dissolution rate and elemental release in ERW scenarios. In experiments conducted over longer timescales and in the field with soils that have been routinely exposed to P-bearing fertilizers, the extent of P removal from solution and thus the impact of P on ERW may differ. The impacts of ERW on plants and on CO_2 removal rates will likely depend on the mineral loading rates used. Interactions with plants will likely impact CO_2 removal rates and further complicate quantification of CO_2 removal (Haque et al., 2019; Kelland et al., 2020), suggesting this is an area requiring further detailed study.

The outcomes observed in laboratory and field scale ERW initiatives will depend heavily upon the soils that are used and how they interact with mineral treatments. However, the addition of mineral treatments may significantly alter soil geochemical behaviour. Because neither mineral-only nor soil-only experiments accurately represent the conditions of enhanced weathering in soils, only mixtures using site-specific soils can be relied upon to provide accurate estimates of weathering rates and CO_2 sequestration capacity.

Acknowledgments

Funding for this research was provided by an NSERC Discovery Grant and a Queen's University Research Initiation grant awarded to ALH. Wollastonite used in this study was graciously provided by Bob Vasily of Canadian Wollastonite. We would like to acknowledge Vasileios Mavromatis, Heather Jamieson, Matthew Leybourne, and the editor, Michael Kersten, and two anonymous reviewers for their insightful comments on this research. The authors would also like to thank Adriana Taylor for assistance in the laboratory, Alexandre Voinot and Marissa Valentino of Queen's University Facility for Isotopic Research for assistance with ICP-OES and TQ-ICP-MS analysis, Agatha Dobosz of Queen's University for assistance with SEM analysis, Karla Newman of the Trent University Water Quality Center for assistance with TQ-ICP-MS analysis, the University of Guelph Agriculture and Food Laboratory for their assistance with solid carbon analysis, and Carole Causserand for assistance with the DIC/DOC analyses.

References

Amann, T. et al., 2020. Enhanced Weathering and related element fluxes–a cropland mesocosm approach. Biogeosciences, 17(1): 103-119.

Anda, M., Shamshuddin, J., Fauziah, C., 2013. Increasing negative charge and nutrient contents of a highly weathered soil using basalt and rice husk to promote cocoa growth under field conditions. Soil and Tillage Research, 132: 1-11.

Anda, M., Shamshuddin, J., Fauziah, C., 2015. Improving chemical properties of a highly weathered soil using finely ground basalt rocks. Catena, 124: 147-161.

Andrews, M.G., Taylor, L.L., 2019. Combating climate change through enhanced weathering of agricultural soils. Elements: An International Magazine of Mineralogy, Geochemistry, and Petrology, 15(4): 253-258.

Appelo, C.A.J., Postma, D., 2004. Geochemistry, groundwater and pollution. CRC press.

Beerling, D.J. et al., 2020. Potential for large-scale CO_2 removal via enhanced rock weathering with croplands. Nature, 583(7815): 242-248.

Berner, R.A., Morse, J.W., 1974. Dissolution kinetics of calcium carbonate in sea water; IV, Theory of calcite dissolution. American Journal of Science, 274(2): 108.

Cipolla, G., Calabrese, S., Noto, L.V., Porporato, A., 2021. The role of hydrology on enhanced weathering for carbon sequestration I. Modeling rock-dissolution reactions coupled to plant, soil moisture, and carbon dynamics. Advances in Water Resources: 103934.

Daval, D., 2018. Carbon dioxide sequestration through silicate degradation and carbon mineralisation: promises and uncertainties. Materials Degradation, 2(1): 1-4.

Dietzen, C., Harrison, R., Michelsen-Correa, S., 2018. Effectiveness of enhanced mineral weathering as a carbon sequestration tool and alternative to agricultural lime: An incubation experiment. International Journal of Greenhouse Gas Control, 74: 251-258.

1156 Fondu, L., Decoster, M., De Bo, I., Van Hulle, S., 2010. Phosphate sorption capacities of
1157 different substrates in view of application in water treatment systems for ponds, 7th
1158 IWA World Water Congress and Exhibition. International Water Association (IWA).
1159 Gaillardet, J., Dupré, B., Louvat, P., Allegre, C., 1999. Global silicate weathering and CO_2
1160 consumption rates deduced from the chemistry of large rivers. Chemical geology,
1161 159(1-4): 3-30.
1162 Golubev, S.V., Pokrovsky, O.S., Schott, J., 2005. Experimental determination of the effect of
1163 dissolved CO_2 on the dissolution kinetics of Mg and Ca silicates at 25 °C. Chemical
1164 Geology, 217(3): 227-238.
1165 Haque, F., Santos, R.M., Chiang, Y.W., 2020. CO_2 sequestration by wollastonite-amended
1166 agricultural soils–An Ontario field study. International Journal of Greenhouse Gas
1167 Control, 97: 103017.
1168 Haque, F., Santos, R.M., Dutta, A., Thimmanagari, M., Chiang, Y.W., 2019. Co-Benefits of
1169 Wollastonite Weathering in Agriculture: CO_2 Sequestration and Promoted Plant
1170 Growth. ACS Omega, 4(1): 1425-1433.
1171 Harley, A.D., Gilkes, R.J., 2000. Factors influencing the release of plant nutrient elements
1172 from silicate rock powders: A geochemical overview. Nutrient Cycling in
1173 Agroecosystems, 56(1): 11-36.
1174 Harrison, A.L., Dipple, G.M., Power, I.M., Mayer, K.U., 2015. Influence of surface
1175 passivation and water content on mineral reactions in unsaturated porous media:
1176 Implications for brucite carbonation and CO_2 sequestration. Geochimica et
1177 Cosmochimica Acta, 148: 477-495.
1178 Harrison, A.L., Dipple, G.M., Power, I.M., Mayer, K.U., 2016. The impact of evolving
1179 mineral–water–gas interfacial areas on mineral–fluid reaction rates in unsaturated
1180 porous media. Chemical Geology, 421: 65-80.

1181 Hartmann, J. et al., 2013. Enhanced chemical weathering as a geoengineering strategy to
1182 reduce atmospheric carbon dioxide, supply nutrients, and mitigate ocean acidification.
1183 Reviews of Geophysics, 51(2): 113-149.
1184 Hayder, A., Vanderburgt, S., Santos, R.M., Chiang, Y.W., 2019. Phosphorous runoff risk
1185 assessment and its potential management using wollastonite according to geochemical
1186 modeling. Open Agriculture, 4(1): 787-794.
1187
1188 Haynes, R.J., Zhou, Y.-F., 2020. Silicate sorption and desorption by a Si-deficient soil–
1189 Effects of pH and period of contact. Geoderma, 365: 114204.
1190 Heaney, P.J., 1993. A proposed mechanism for the growth of chalcedony. Contributions to
1191 Mineralogy and Petrology, 115(1): 66-74.
1192
1193 IPCC, 2018. Global warming of 1.5 °C. An IPCC Special Report on the impacts of global
1194 warming of 1.5 °C.
1195 Jakobsen, S.T., 1979. Interaction between phosphate and calcium in nutrient uptake by plant
1196 roots. Communications in Soil Science and Plant Analysis, 10(1-2): 141-152.
1197 James, R.H. et al., 2020. Carbon Dioxide Removal via Enhanced Rock Weathering With
1198 Agriculture in Large-Scale Field Trials, AGU Fall Meeting Abstracts, pp. B003-0002.
1199 Jariwala, H., Haque, F., Vanderburgt, S., Santos, R.M., Chiang, Y.W., 2022. Mineral–Soil–
1200 Plant–Nutrient Synergisms of Enhanced Weathering for Agriculture: Short-Term
1201 Investigations Using Fast-Weathering Wollastonite Skarn. Frontiers in Plant Science,
1202 13.
1203
1204 Kelland, M.E. et al., 2020. Increased yield and CO_2 sequestration potential with the C4 cereal
1205 Sorghum bicolor cultivated in basaltic rock dust-amended agricultural soil. Global
1206 Change Biology, 26(6): 3658-3676.
1207 Lee, Y.B., Kim, P.J., 2007. Reduction of phosphate adsorption by ion competition with
1208 silicate in soil. Korean Journal of Environmental Agriculture, 26(4): 286-296.
1209 Manning, D.A.C., Renforth, P., Lopez-Capel, E., Robertson, S., Ghazireh, N., 2013.
1210 Carbonate precipitation in artificial soils produced from basaltic quarry fines and

composts: An opportunity for passive carbon sequestration. International Journal of Greenhouse Gas Control, 17: 309-317.

McDermott, F., Barros, R., Cooper, M., 2019. An investigation of waste basalt (quarry dust) as a soil amendment to sequester atmospheric CO_2, Geophysical Research Abstracts.

Mkhonza, N.P., Buthelezi-Dube, N.N., Muchaonyerwa, P., 2020. Effects of lime application on nitrogen and phosphorus availability in humic soils. Scientific Reports, 10(1): 8634.

National Academies of Sciences, Board, O.S., 2019. Negative emissions technologies and reliable sequestration: A research agenda.

Obihara, C., Russell, E., 1972. Specific adsorption of silicate and phosphate by soils. Journal of Soil Science, 23(1): 105-117.

Palandri, J.L., Kharaka, Y.K., 2004. A compilation of rate parameters of water-mineral interaction kinetics for application to geochemical modeling, Geological Survey Menlo Park CA.

Panday, K., Prasad, G., Singh, V., 1986. Use of wollastonite for the treatment of Cu (II) rich effluents. Water, Air, and Soil Pollution, 27(3): 287-296.

Parkhurst, D.L., Appelo, C., 2013. Description of input and examples for PHREEQC version 3: a computer program for speciation, batch-reaction, one-dimensional transport, and inverse geochemical calculations. 2328-7055, US Geological Survey.

Peters, S.C., Blum, J.D., Driscoll, C.T., Likens, G.E., 2004. Dissolution of wollastonite during the experimental manipulation of Hubbard Brook Watershed 1. Biogeochemistry, 67(3): 309-329.

Pogge von Strandmann, P.A.E., Tooley, C., Mulders, J.J.P.A., Renforth, P., 2022. The Dissolution of Olivine Added to Soil at 4°C: Implications for Enhanced Weathering in Cold Regions. Frontiers in Climate, 4.

1237 Pokrovsky, O.S., Shirokova, L.S., Benezeth, P., Schott, J., Golubev, S.V., 2009. Effect of
1238 organic ligands and heterotrophic bacteria on wollastonite dissolution kinetics.
1239 American Journal of Science, 309(8): 731-772.
1240 Power, I.M. et al., 2013. Carbon mineralization: from natural analogues to engineered
1241 systems. Reviews in Mineralogy and Geochemistry, 77(1): 305-360.
1242 Power, I.M. et al., 2021. Carbonation, Cementation, and Stabilization of Ultramafic Mine
1243 Tailings. Environmental Science & Technology, 55(14): 10056-10066.
1244 Renforth, P., Pogge von Strandmann, P.A.E., Henderson, G.M., 2015. The dissolution of
1245 olivine added to soil: Implications for enhanced weathering. Applied Geochemistry,
1246 61: 109-118.
1247 Rosen, C.J., Kelling, K.A., Stark, J.C., Porter, G.A., 2014. Optimizing Phosphorus Fertilizer
1248 Management in Potato Production. American Journal of Potato Research, 91(2): 145-
1249 160.
1250 Roy, A.C., Ali, M.Y., Fox, R.L., Silva, J.A., 1971. Influence of calcium silicate on phosphate
1251 solubility and availability in Hawaiian Latosols, Symposium on soil fertility and
1252 evaluation. University of Hawaii New Delhi, pp. 756-765.
1253 Schott, J. et al., 2012. Formation, growth and transformation of leached layers during silicate
1254 minerals dissolution: The example of wollastonite. Geochimica et Cosmochimica
1255 Acta, 98: 259-281.
1256 Schuiling, R., Krijgsman, P., 2006. Enhanced weathering: an effective and cheap tool to
1257 sequester CO_2. Climatic Change, 74(1): 349-354.
1258 Shao, S. et al., 2016. Long-term responses in soil solution and stream-water chemistry at
1259 Hubbard Brook after experimental addition of wollastonite. Environmental
1260 Chemistry, 13(3): 528-540.

Sharma, Y., Gupta, G., Prasad, G., Rupainwar, D., 1990. Use of wollastonite in the removal of Ni (II) from aqueous solutions. Water, Air, and Soil Pollution, 49(1): 69-79.

Sigua, G.C., Stone, K.C., Bauer, P.J., Szogi, A.A., Shumaker, P.D., 2017. Impacts of irrigation scheduling on pore water nitrate and phosphate in coastal plain region of the United States. Agricultural Water Management, 186: 75-85.

Swamy, V., Saxena, S.K., Sundman, B., Zhang, J., 1994. A thermodynamic assessment of silica phase diagram. Journal of Geophysical Research: Solid Earth, 99(B6): 11787-11794.

Taylor, L.L. et al., 2021. Increased carbon capture by a silicate-treated forested watershed affected by acid deposition. Biogeosciences, 18(1): 169-188.

Ten Berge, H.F. et al., 2012. Olivine weathering in soil, and its effects on growth and nutrient uptake in ryegrass (Lolium perenne L.): a pot experiment.

Tubana, B.S., Babu, T., Datnoff, L.E., 2016. A review of silicon in soils and plants and its role in US agriculture: history and future perspectives. Soil Science, 181(9/10): 393-411.

Washbourne, C.-L., Lopez-Capel, E., Renforth, P., Ascough, P.L., Manning, D.A.C., 2015. Rapid Removal of Atmospheric CO_2 by Urban Soils. Environmental Science & Technology, 49(9): 5434-5440.

Zhang, G., Kang, J., Wang, T., Zhu, C., 2018. Review and outlook for agromineral research in agriculture and climate mitigation. Soil Research, 56(2): 113-122.